AD-769 637

A DYNAMIC SIMULATION OF SOIL-WHEEL INTERACTION

STEVENS INSTITUTE OF TECHNOLOGY

PREPARED FOR

ARMY TANK-AUTOMOTIVE COMMAND

SEPTEMBER 1973

Distributed By:

NTIS

National Technical Information Service
U. S. DEPARTMENT OF COMMERCE

UNCLASSIFIED

Security Classification

AD 769637

DOCUMENT CONTROL DATA - R & D

(Security classification of title, body of abstract and indexing annotation must be entered when the overall report is classified)

1. ORIGINATING ACTIVITY (Corporate author)

Davidson Laboratory, Stevens Institute of Technology
Hoboken, New Jersey 07030

2a. REPORT SECURITY CLASSIFICATION

UNCLASSIFIED

2b. GROUP

3. REPORT TITLE

A DYNAMIC SIMULATION OF SOIL-WHEEL INTERACTION

4. DESCRIPTIVE NOTES (Type of report and inclusive dates)

Final Report

5. AUTHOR(S) (First name, middle initial, last name)

Sheridan Lee Miszklevitz

6. REPORT DATE

September 1973

7a. TOTAL NO. OF PAGES

~~x + 63~~ 77

7b. NO. OF REFS

15

8a. CONTRACT OR GRANT NO.

DAAE-07-73-C-0131

b. PROJECT NO.

DL Project 4047/414

c.

d.

9a. ORIGINATOR'S REPORT NUMBER(S)

SIT-DL-73-1689

9b. OTHER REPORT NO(S) (Any other numbers that may be assigned this report)

10. DISTRIBUTION STATEMENT

Distribution of this document is unlimited.

11. SUPPLEMENTARY NOTES

12. SPONSORING MILITARY ACTIVITY

U. S. Army Tank-Automotive Command
Warren, Michigan 48090

13. ABSTRACT

A dynamic vehicle model, simulating both the vehicle dynamics and the wheel-soft soil interaction, is presented. Equations of motion are presented for a two-dimensional, six-degree-of-freedom vehicle. Relationships for forces and moments on the vehicle and its wheels due to wheel-soil interaction are developed as functions of normal and shear stresses in the soil. Both the rigid wheel and flexible wheel cases are addressed. Current state-of-the-art relationships among shear stress, normal stress, wheel sinkage, and wheel slip are used. Parametric studies are used to assess the qualitative validity of the model.

While experimental data does not exist, comparison of the results of the simulation with known information from the field of off-the-road mobility indicates the model to be valid.

Reproduced by
NATIONAL TECHNICAL
INFORMATION SERVICE
U S Department of Commerce
Springfield VA 22151

1a

DD FORM 1 NOV 65 1473 (PAGE 1)

S/N 0101-807-6811

UNCLASSIFIED

Security Classification

A-31454

UNCLASSIFIED
Security Classification

14. KEY WORDS	LINK A ROLE	LINK A WT	LINK B ROLE	LINK B WT	LINK C ROLE	LINK C WT
LAND LOCOMOTION						
COMPUTER SIMULATION						
SOIL-VEHICLE INTERFACE						

14

DD FORM 1 NOV 65 1473 (BACK)

S/N 0101-807-6821

UNCLASSIFIED
Security Classification

4-31409

DAVIDSON LABORATORY
Stevens Institute of Technology
Castle Point Station
Hoboken, N. J. 07030

Report SIT-DL-73-1689

September 1973

A DYNAMIC SIMULATION OF SOIL-WHEEL INTERACTION

by

Sheridan Lee Miszklevitz

Prepared for
U. S. Army Tank-Automotive Command
under
Contract DAAE07-73-C-0131
(DL Project 4047/414)

This document has been approved for public release and sale; its distribution is unlimited. Application for copies may be made to the Defense Documentation Center, Cameron Station, 5010 Duke Street, Alexandria, Virginia 22314. Reproduction of the document in whole or in part is permitted for any purpose of the United States Government.

Approved

I. Robert Ehrlich, Manager
Transportation Research Group

x + 63 pages
21 figures

ic

ABSTRACT

A Dynamic Simulation of Soil-Wheel Interaction

by

Sheridan L. Hiszklevits

Advisor

I. Robert Ehrlich

May 1973

A dynamic vehicle model, simulating both the vehicle dynamics and the wheel-soft soil interaction, is presented. Equations of motion are presented for a two-dimensional, six-degree-of-freedom vehicle. Relationships for forces and moments on the vehicle and its wheels due to wheel-soil interaction are developed as functions of normal and shear stresses in the soil. Both the rigid wheel and flexible wheel cases are addressed. Current state-of-the-art relationships among shear stress, normal stress, wheel sinkage, and wheel slip are used. Parametric studies are used to assess the qualitative validity of the model.

While experimental data does not exist, comparison of the results of the simulation with known information from the field of off-the-road mobility indicates the model to be valid.

TABLE OF CONTENTS

Abstract ii

List of Symbols v

List of Figures ix

List of Tables x

I. INTRODUCTION 1

II. BACKGROUND 2

A. Predicting Wheel Performance 2

B. Vehicle Simulation 7

III. THE MATHEMATICAL MODEL 12

A. The Vehicle and its Reference Frames 12

B. Equations of Motion 14

1. Hull Equations 14

2. Wheel Equations 15

C. Soil Forces on a Rigid Wheel 16

1. Normal Stress Forces and Moments on a Rigid Wheel 16

2. Shear Stress Forces and Moments on a Rigid Wheel . 21

D. Normal and Shear Stress Functions 24

E. Integration of the Soil Force and Moment Equations for the Rigid Wheel 31

1. Integrations Involving Normal Stress 31

2. Integrations Involving Shear Stress 32

F. Soil Forces on a Flexible Wheel 34

1. Tire Deflection 34

2. Normal Stress Forces and Moments on a Flexible Wheel 37

3. Shear Stress Forces and Moments on a Flexible Wheel 41

G. Integration of the Soil Force and Moment Equations for the Flexible Wheel 46

1. Integrations Involving Normal Stress 46

2. Integrations Involving Shear Stress 47

H. Equations of Motion in the Simulation 47

IV. THE SIMULATION 50

A. General 50

B. Concept 50

C. Description 50

V. QUALITATIVE VALIDATION 54

VI. CONCLUSIONS AND RECOMMENDATIONS 60

A. Conclusion 60

B. Recommendations 60

REFERENCES 61

ACKNOWLEDGEMENTS 63

VITA 64

LIST OF SYMBOLS

A, B, C	coefficients in assumed normal stress equation
α	the angle between a normal force on the wheel and the Z axis; the angle between a tangential force on the wheel and the X axis
α'	the angle between the Z axis and the centerline of the zone of tire deflection
β	the angle from the x axis to the center of the theoretical contact patch
B	the width of a soil sinkage plate
b	wheel width
c	soil cohesion
D_1, D_2	suspension forces on front and rear wheels, respectively
d	distance in Z direction from a wheel X axis
F_x, F_z	the net forces on a wheel in the X and Z directions
F_{x1}	the net force on the front wheel in the X direction
F_{x2}	the net force on the rear wheel in the X direction
F_{z1}	the net force on the front wheel in the Z direction
F_{z2}	the net force on the rear wheel in the Z direction
F_{XN}, $F_{x\sigma}$	the X component of normal force on a wheel
F_{ZN}, $F_{z\sigma}$	the Z component of normal force on a wheel
F_{XT}, $F_{x\tau}$	the X component of shear force on a wheel
F_{ZT}, $F_{z\tau}$	the Z component of shear force on a wheel
$F_{cz\sigma}$	the force due to normal stress on the deflected portion of a contact patch
$F_{cz\tau}$	the force due to shear stress on the deflected portion of a contact patch
$F_{cz\sigma x}$	the X component of $F_{cz\sigma}$

$F_{cz\sigma z}$	the Z component of $F_{cz\sigma}$
$F_{cz\tau x}$	the X component of $F_{cz\tau}$
$F_{cz\tau z}$	the Z component of $F_{cz\tau}$
G_y	the net torque on the body about the Y axis
G_{yw}	the combined net torque on both front and rear wheels
γ	the wheel angle, measured from the horizontal, which locates points on the wheel surface
γ_1	the wheel entrance angle; where it first touches the soil
γ_2	the wheel exit angle; where it leaves the soil
γ_{1o}	the entrance angle to the undisturbed soil profile
γ_{2o}	the exit angle to the undisturbed soil profile
γ_{1p}, γ_{2p}	the angles which define the limits of the zone of tire deflection for a flexible wheel
$\gamma_{\frac{1}{2}}$	the angle to the center of the actual contact patch
$\gamma_{\frac{1}{2}p}$	the angle to the center of the deflected portion of the contact patch
H	a vertical load on a wheel
h	the initial soil bearing capacity, dependent on plate shape
I_x, I_y, I_z	moments of inertia of a body about the X, Y, and Z axes
I_{xz}	the product of inertia of a body about the X and Z axes
I_{yw}	the combined wheel-drive train rotary moment of inertia
j	soil deformation under shear stress
k_c	Bekker's soil modulus of cohesion
k_ϕ	Bekker's soil modulus of friction
k_c'	Sela-Ehrlich modified soil modulus of cohesion
K	the deformation modulus of a soil shear stress-strain curve
L	the length of a linear contact patch

M	vehicle mass
m_1, m_2	mass of front and rear wheels, respectively
M_x	the total moment at the vehicle CG due to soil forces in the X direction
$M_{x\sigma}$, $M_{x\tau}$	the moment at the vehicle CG due to $F_{x\sigma}$ and $F_{x\tau}$
$M_{\tau 1}$, $M_{\tau 2}$	the moment at the front and rear wheel centers due to shear stress
M'	the moment at the vehicle CG due to $F_{cz\sigma x}$
M''	the moment at the vehicle CG due to $F_{cz\tau x}$
M_{w1}, M_{w2}	the engine torque on the front and rear wheels
N	the normal soil force on a wheel
n	Bekker's soil sinkage exponent
σ	normal soil stress (pressure)
σ_{max}	the maximum normal pressure whech occurs under a rigid wheel
σ_{maxTH}	the theoretical maximum normal pressure which would occur if a wheel were rigid
ϕ	the angle of internal soil friction
p'	the maximum allowable soil pressure under a flexible wheel
P_i	the inflation pressure within a tire
P_c	the carcass pressure of a tire
p	normal soil stress (pressure)
P_i	the initial soil bearing capacity
P,Q,R	rates of rotation of a body about the X, Y, and Z axes
R_h	hydraulic radius
r	radius of a wheel
s	wheel slip
T	the tangential soil force on a wheel

τ	shear stress
θ	pitch angle of a body measured about the Y axis
θ_G	the local ground slope at a wheel
U, V, W	velocities in the X, Y, and Z directions
W'	vehicle weight
w_1, w_2	weight of front and rear wheels
z	depth of sinkage
z_i	the degree of soil compaction, dependent on previous loads on the soil
z_m	depth of wheel sinkage at the center of the contact patch
z_{mTH}	the theoretical depth of wheel sinkage which would occur if a wheel were rigid
Z_{Ri}	the "rest" position of a wheel (i = 1, 2 for front or rear)
Z_i	the wheel displacement from the rest position (i = 1,2 for front or rear wheel)

LIST OF FIGURES

1. Forces Acting on a Rigid Wheel 3

2. Soil Pressure Distribution Under a Rigid Wheel 4

3. Triangular Normal Stress Distribution in Schuring-Belsdorf Model 8

4. Idealized Relationship Between Front Angle and Rear Angle of Pneumatic Tires in Schuring-Belsdorf Model 8

5. Idealized Contact Patch and Sinkage Relationship in Muddappa-Baker Model 10

6. Simulation Coordinate Systems 13

7. Normal Stress Under a Rigid Wheel 17

8. Moment at Vehicle Center of Gravity Due to Soil Forces in X-Direction 20

9. Shear Stress Under a Rigid Wheel 22

10. Assumed Normal Stress Distribution 25

11. Local Ground Slope and Sinkage for a Rigid Front Wheel 25

12. Experimental Pressure vs Sinkage Curves From Repetitive Loading 28

13. Normal Stress Distribution Under a Rear Wheel 29

14. Normal Stress Distribution Under a Flexible Wheel 36

15. Normal Stress Under a Flexible Wheel 38

16. Shear Stress Under a Flexible Wheel 42

17. Shear Stress Distribution Under a Deflected Tire 43

18. Forces and Moments on the Vehicle and Wheels 48

19. Program Subroutines 51

20. Plot of Vehicle Velocity vs Time for Various k_ϕ 57

21. Plot of Vehicle Velocity vs Time for Various Slopes 59

LIST OF TABLES

1. Comparison of Numerical Integration Methods 33

2. Vehicle Velocity at Selected Times for Various k_ϕ 56

3. Vehicle Velocity at Selected Times for Various Slopes ... 58

I. INTRODUCTION

The computer has provided a valuable tool for use in the planning, development, and analysis of off-the-road vehicle systems; cut-and-try techniques are giving way to computerized simulations as a method of analyzing various systems in the search for the optimum configuration. It appears likely that long procurement lead times, and their associated skyrocketing costs, can be reduced through the use of simulations.

A detailed dynamic model which includes vehicle dynamics and wheel-soft soil relationships is necessary to realize the full potential of the computer, and to provide accurate modeling of prototypes. While they have taken the necessary early steps, previously developed simulations are not detailed dynamic models; one type depends upon equilibrium equations [1,2], another upon rigid wheel-rigid surface relationships [3], while a third models the vehicle components and determines soil forces from a data bank of experimental results[4]. This report is a significant deviation from most previous work in that it presents a dynamic vehicle model with particular emphasis on the wheel-soil interaction. The approach to the wheel-soil problem considers the basic shear and normal stresses acting at the soil-wheel interface, and derives all forces and moments as functions of these stresses. Current state-of-the-art relationships among shear stress, normal stress, sinkage, and wheel slip are used. In this analysis, speed effects have been neglected, since current literature indicates no velocity effects in the range of consideration.

II. BACKGROUND

A. PREDICTING WHEEL PERFORMANCE

The validity of any mathematical simulation depends upon the ability to formulate the relationships among the factors which determine the behavior of the prototype. Of interest in the soil-wheel problem are the relationships among shear and normal stresses within the soil, forces on the wheel, and wheel slip. The formulation of these relationships has proven to be particularly difficult.

The forces acting at the soil-wheel interface are shown in Figure 1. Shear and normal stresses each produce component forces in the horizontal and vertical directions. The total horizontal and vertical forces are the sums of these components.

One of the most widely accepted expressions for pressure under a plate in soil is that proposed by Bekker [5]:

$$p = \left(\frac{k_c}{B} + k_\phi\right) z^n \tag{1}$$

where

p = soil pressure on the plate

k_c, k_ϕ, and n are soil parameters

B = width of the plate

z = depth of sinkage of the plate

Bekker used Equation (1) to predict the sinkage of a rigid wheel in soft soil from data obtained using plate tests.

Figure 2 shows a typical normal soil pressure distribution that has been measured under a rigid wheel. Also shown is the pressure

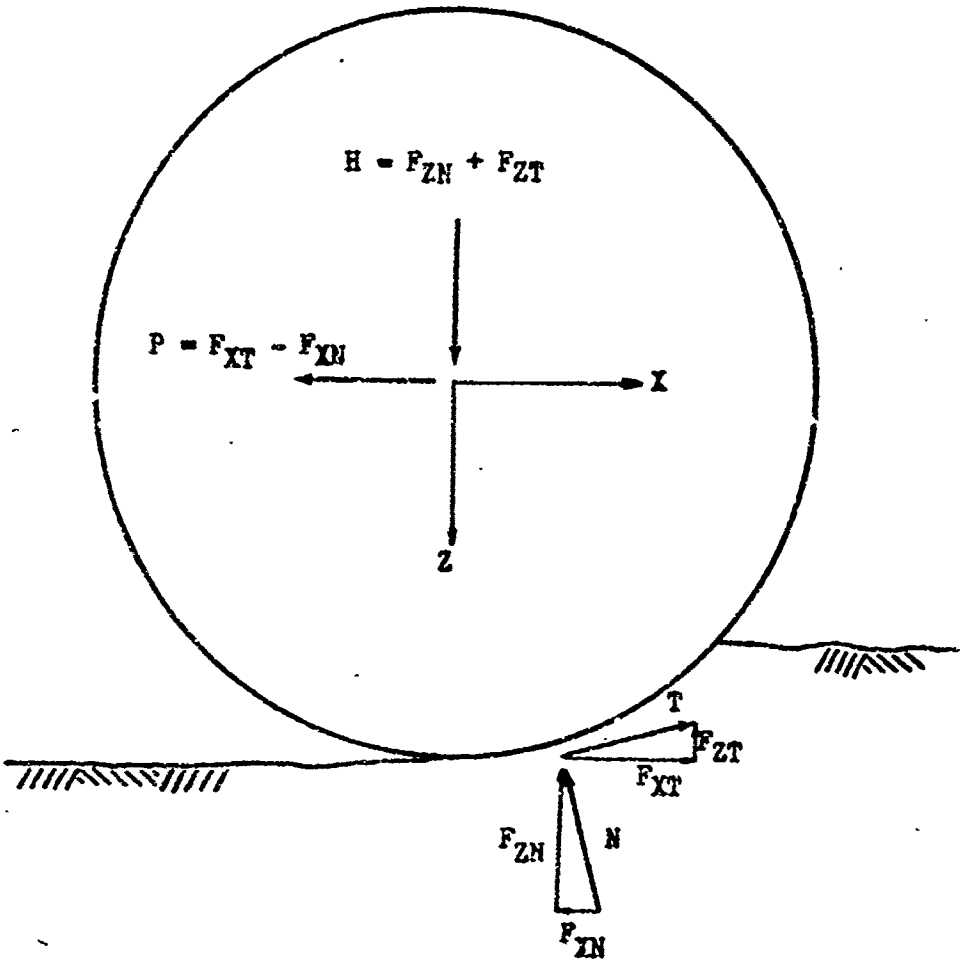

FIGURE 1 FORCES ACTING ON A RIGID WHEEL

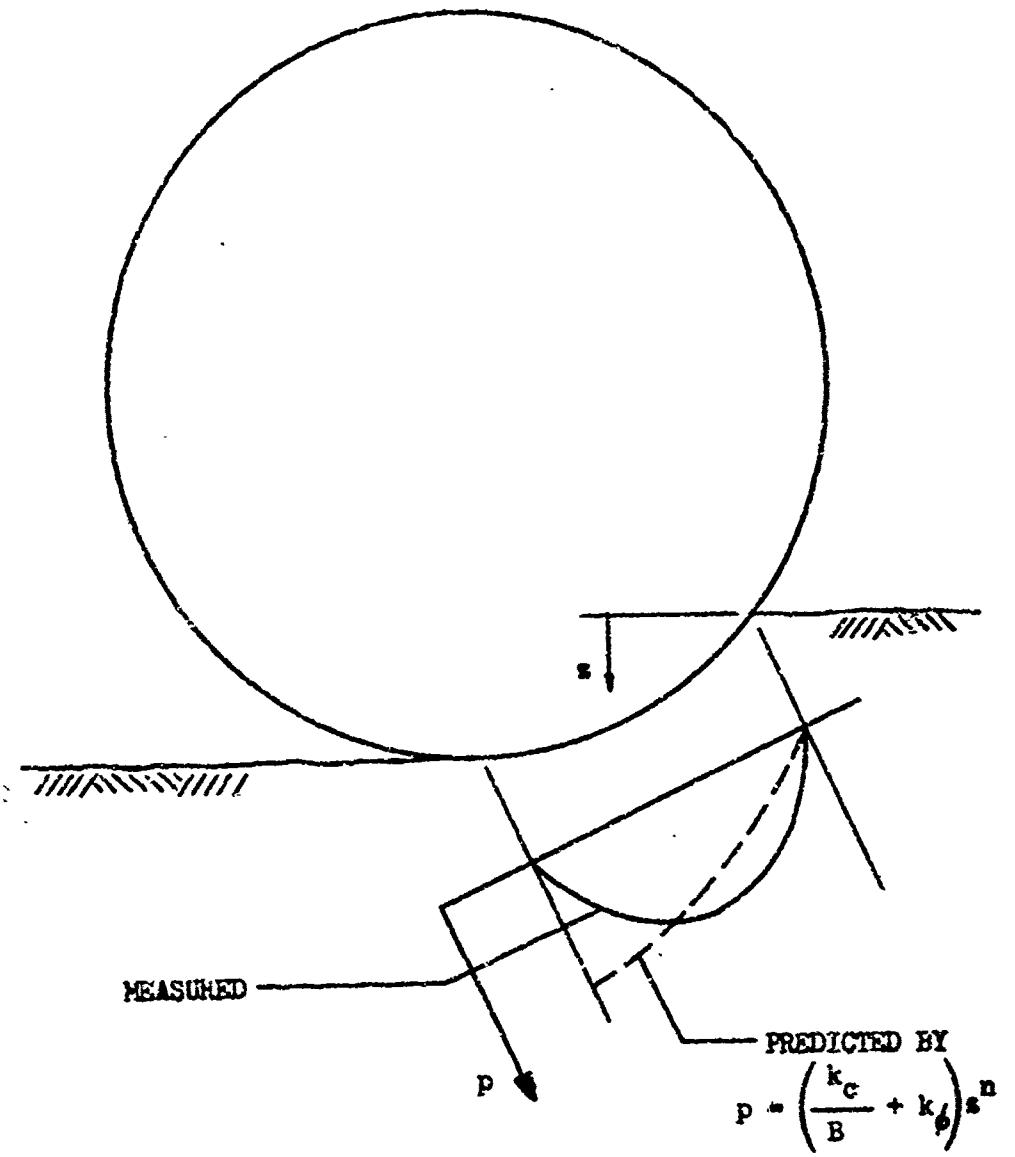

FIGURE 2 SOIL PRESSURE DISTRIBUTION UNDER A RIGID WHEEL

distribution predicted by Bekker's equation. The significant differences are evident. As can easily be seen, the lift force predicted by using Equation (1) will be larger than the actual force realized, hence the predicted sinkage will be less than the actual sinkage.

Sela and Ehrlich [6] recently proposed a modification to Bekker's equation:

$$p = p_i + \frac{h}{R_h} + \left(k_\phi + \frac{k_c'}{R_h}\right)(z_i + z)^n \qquad (2)$$

where

p = the nominal soil pressure under a plate

p_i = the initial soil bearing capacity, independent of plate shape (a parameter of the soil)

h = the initial soil bearing capacity, dependent on plate shape (a parameter of the soil)

R_h = hydraulic radius of the plate = $\frac{\text{plate area}}{\text{plate perimeter}}$

k_ϕ = the soil strength modulus, independent of plate shape (a parameter of the soil)

k_c' = the soil strength modulus, dependent on plate shape (a parameter of the soil)

z_i = the degree of soil compaction, dependent on previous loads on the soil (a parameter of the soil)

z = the sinkage into the soil at which the nominal pressure, p, is measured

n = the soil sinkage exponent (a parameter of the soil)

They then used Equation (2) to predict the performance of a rigid wheel in soft soil at zero slip [7]. Sela and Ehrlich attempted to compensate for the difference in actual and predicted pressure distributions by neglecting the shear stress contribution to normal force on the wheel.

The performance predicted has shown good agreement with experimental results.

The well-known Coulomb equation [8] gives the shear strength of a soil:

$$\tau = (c + \sigma \tan\phi) \tag{3}$$

where

τ = shear strength (maximum available shear stress)

c = soil cohesion

σ = normal pressure on the soil

ϕ = angle of internal soil friction

Using Equation (3), Janosi and Hanamoto [9] proposed the following equation to describe a soil shear stress-strain curve:

$$\tau = (c + \sigma \tan\phi)(1 - e^{-j/K}) \tag{4}$$

where

e = the base for Naperian logarithms

j = the soil deformation

K = the deformation modulus of the soil shear stress-strain curve

As applied to a loaded soil-shear plate, this equation states that to displace the plate a distance j, the shear stress τ must be overcome. Note that this is less than the maximum shear strength given by Equation (3), and that for very large deformations ($j \rightarrow \infty$), Equation (4) approaches Coulomb's equation.

In extending this equation to predict shear stress distribution under a wheel, Janosi [10] assumed that the wheel contact patch was a series of small plates that acted independently, and obtained an

expression for j from the cycloidal movement of the wheel periphery.

Several other theories regarding shear stress have been advanced, but they fall into two categories:

(1) the solutions are incomplete because the number of unknowns exceeds the number of equations which can be written.

(2) if complete, the solution is limited to a very special soil condition.

Accordingly, Janosi's original approach is still the one used by many researchers.

It is believed that sinkage and normal stress are functions of wheel slip. However, these relationships have not yet been discovered.

B. VEHICLE SIMULATION

In an extensive report on vehicle-terrain simulations, Schuring and Belsdorf [1] have presented a model of a vehicle traversing soft, smooth soil. The simulation assumed steady-state movement, and hence was postulated in terms of equations of equilibrium.

The wheel performance equations were derived from an assumed triangular distribution of normal stress, with the maximum stress determined by Bekker's equation; from the Janosi-Hanamoto equations for shear stress distribution (simplified by some assumptions involving the relative magnitudes of sines and cosines); and from an assumed empirical relationship between leading and trailing portions of the contact zone. See Figures 3 and 4.

Execution of the simulation requires simultaneous solution of various algebraic equations, and provides the following output:

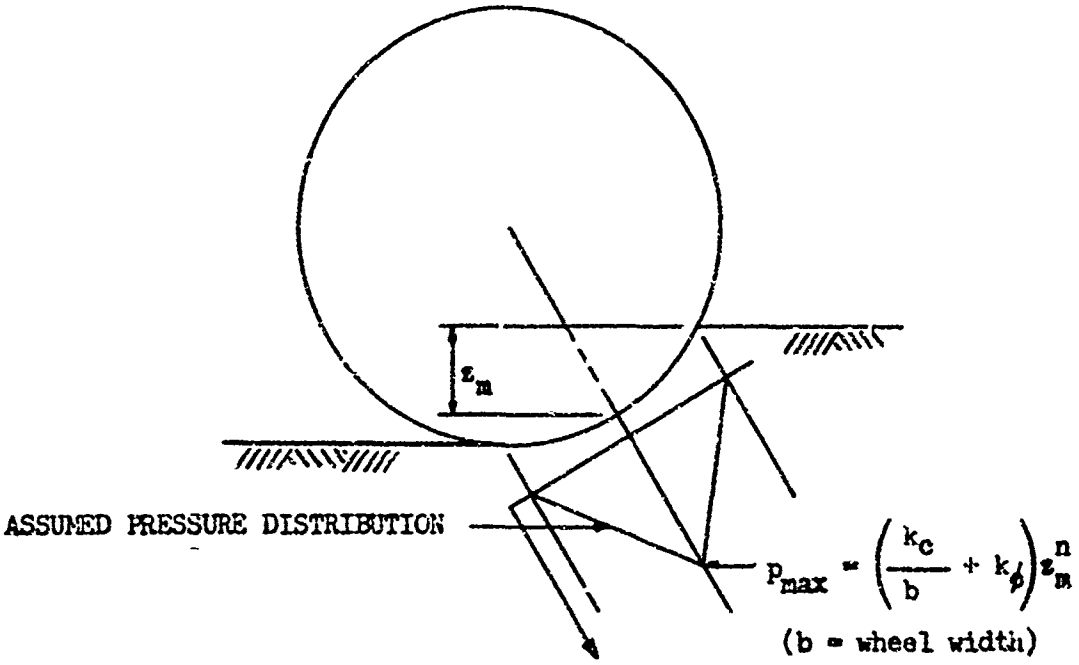

FIGURE 3 TRIANGULAR NORMAL STRESS DISTRIBUTION IN SCHURING-BELSDORF MODEL

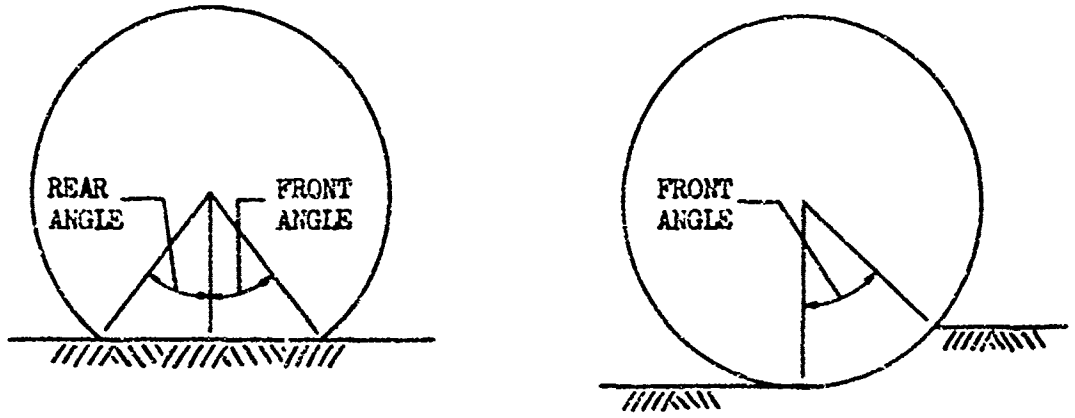

FRONT ANGLE = REAR ANGLE

SOFT WHEEL ON RIGID GROUND

REAR ANGLE = 0

RIGID WHEEL ON SOFT GROUND

FIGURE 4 IDEALIZED RELATIONSHIP BETWEEN FRONT ANGLE AND REAR ANGLE OF PNEUMATIC TIRES IN SCHURING-BELSDORF MODEL

- the "thrust" force at the contact zone of a driven wheel
- the drive torque at the axle of a driven wheel
- the slip of the driven wheel
- the forward velocity of the vehicle

The model, however, has not been verified by experiment.

In the report of their study of egress performance of vehicles, Muddappa and Baker [2] have presented a model of a vehicle traversing soft, smooth soil. The simulation determined inertial forces acting on the vehicle as a result of its velocity, and assumed the vehicle and forces acting on it to be in dynamic equilibrium (steady-state) at finite increments of time. The simulation was postulated in terms of a highly non-linear set of differential equations.

The wheel performance equations were derived from an assumed linear contact patch; from the wheel sinkage given by Equation (1); and from the "compactic resistance" of the soil, computed by integrating Equation (1). See Figure 5.

Execution of the simulation consists of an iterative procedure, and provides the position of the vehicle as part of its output. The model also has not been verified by experiment.

Schoch and Shah [4], in their report on the development of computer-modeling techniques, have presented an example model of a tracked vehicle traversing a soil terrain. This simulation used extensive models of vehicle components and their interaction to calculate engine torque and speed of wheel sprockets.

The track performance was determined from a table of test values for a similiar vehicle. Using sprocket speeds as input, and

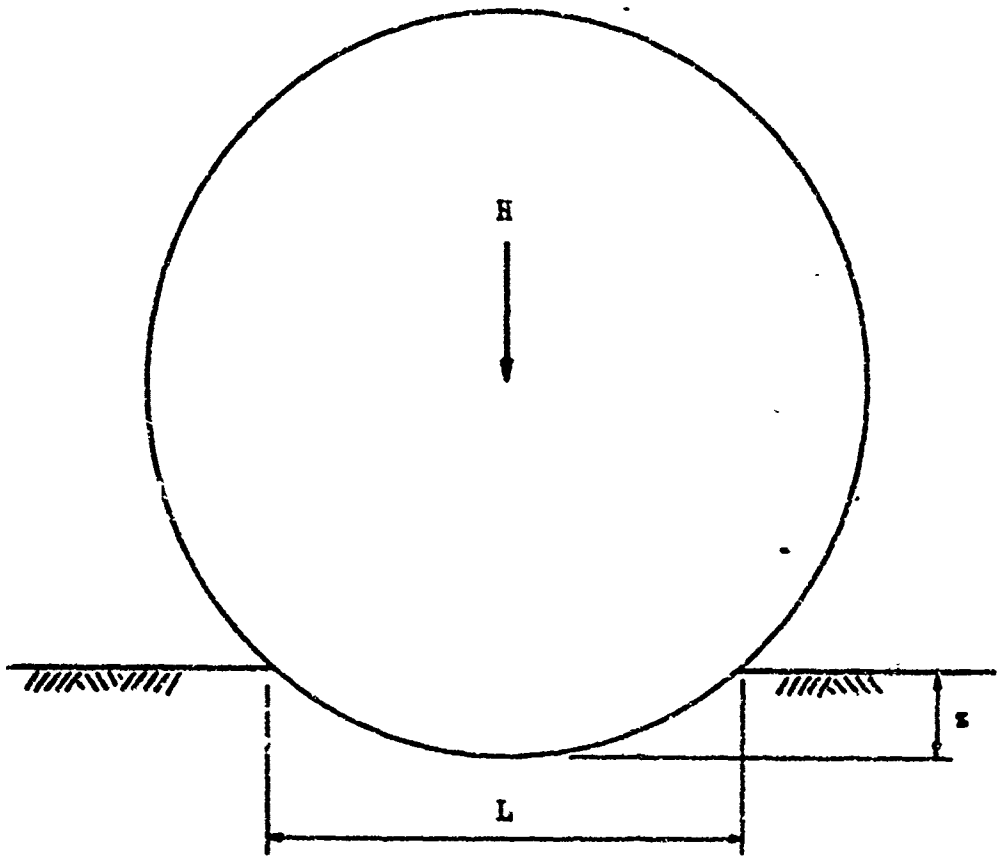

H = the load transmitted to the ground

b = the wheel width

A = wheel contact area = 0.85 L b

$$p = \frac{H}{A}$$

$$z = \left[\frac{p}{\frac{k_c}{b} + k_\phi}\right]^{1/n}$$

FIGURE 5 IDEALIZED CONTACT PATCH AND SINKAGE RELATIONSHIP IN MUDDAPPA-BAKER MODEL

considering factors such as slope, rolling resistance, and soil conditions, the model determines sprocket forces as its output. Vehicle speed follows as a function of sprocket forces.

Sloss, Ehrlich, and Worden [3] have presented a model of a vehicle egressing from water onto a hard ramp. The simulation assumed the vehicle to be in non-steady-state motion, and was postulated in terms of its differential equations of motion. Since the simulation assumed a hard bank, the wheel performance equations derived used normal forces and the coefficient of friction to determine wheel-bank forces. Execution of the simulation involved solving the differential equations of motion by a numerical method, with outputs of vehicle location, speed, acceleration, and pitch attitude. The computer model was verified by scale model tests and has shown close agreement with experimental results.

III. THE MATHEMATICAL MODEL

A. THE VEHICLE AND ITS REFERENCE FRAMES

The simulation discussed in this report uses the US Army M151A1 ¼ Ton Truck, or "Jeep", as its prototype vehicle. The vehicle is assumed to be two-dimensional (vertical plane) with 6 degrees of freedom. The hull of the vehicle has freedom of surge, heave, and pitch*. Each wheel is free to heave. In addition, the front and rear wheels are free to rotate, but they are not independent because of the action of the transfer case.

There are three coordinate systems used in the simulation; they are shown in Figure 6. The X'Z' system is the inertial reference frame, with the X' axis lying along the horizontal. The XZ system is affixed to the vehicle, with its origin at the vehicle center of gravity. When the vehicle is at rest on a horizontal profile, the X axis is horizontal. The xz system is affixed to the hub of each wheel, and carries a subscript which denotes the specific wheel which it describes (1 = Front, 2 = Rear). The xz axes are parallel to the respective XZ axes. Note that since the wheel is only free to heave, the x axis will not be used in this model.

The vehicle suspension is simulated by a spring and damper system. Since there is generally very little movement of wheels in the horizontal direction, the suspension is assumed to be solidly affixed to the

---

*Surge is forward motion; heave is up-and-down motion; and pitch is rotation about an axis which goes through the center of gravity of the vehicle, and is perpendicular to the plane of the vehicle.

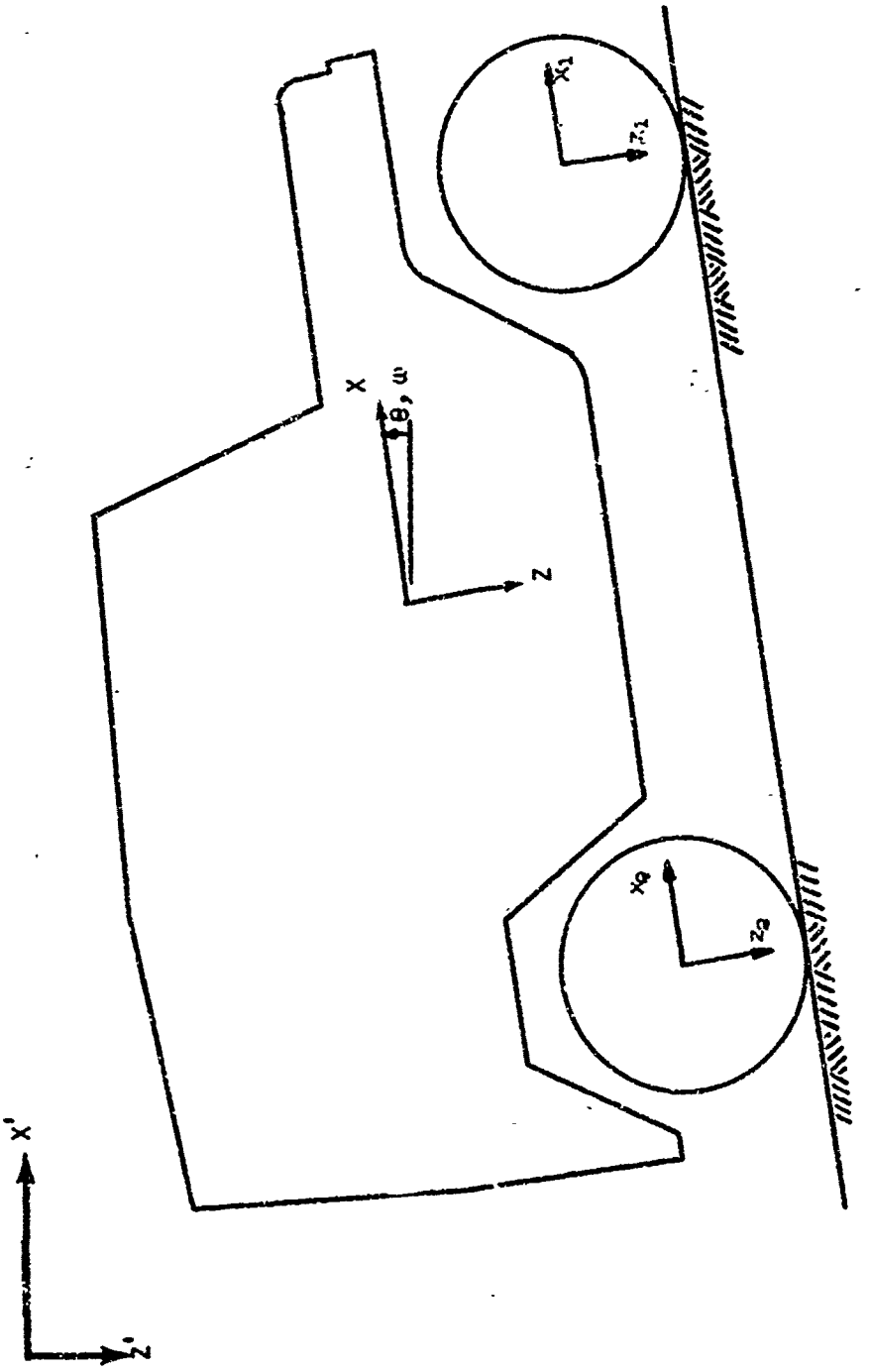

FIGURE 6 SIMULATION COORDINATE SYSTEMS

vehicle with no freedom of movement in the X direction.

B. EQUATIONS OF MOTION

To represent properly the acceleration, velocity, and location of a vehicle undergoing movement, we must rely upon time-dependent equations of motion. These equations for a rigid body have been derived many times before [11], so their derivation is omitted here. Instead, they are presented in the generally accepted form, with comments as to how they are applied to the model.

The equations used in this simulation are the minimum required for program debugging and initial model validation. In reality, wheels accelerating with respect to the body will produce inertial forces on the body. These forces have been neglected since this is a first-cut model designed to perform on uniformly sloping soil with uniform strength (hence, nearly equal wheel sinkages). Under these circumstances, the inertial forces mentioned are small. They must be included later, if, for example, the model is used to study obstacle climbing.

1. Hull Equations

Six degrees of freedom of a solid body give rise to six equations of motion. Of these six, the equations for surge, heave, and pitch are:

Surge: $F_x = M(\dot{U} + QW - RV)$ (5)

Heave: $F_z = M(\dot{W} + PV - QU)$ (6)

Pitch: $G_y = I_y\dot{Q} - P(I_zR - I_{xz}P) + R(I_xP - I_{xz}R)$ (7)

where

U,V,W = velocities in the X, Y, and Z directions

P,Q,R = rates of rotations about the X,Y, and Z axes

M = the mass of the body

F_x,F_z = the net forces on the body in the X and Z directions

I_{xz} = the product of inertia of the body about the X and Z axes

G_y = the net torque on the body about the Y axis

I_x,I_y,I_z = moments of inertia of the body about the X,Y, and Z axes

Under the two-dimensional assumption, the terms V,P, and R are zero, so the equations reduce to the following:

$$F_x = M(\dot{U} + QW) \tag{8}$$

$$F_z = M(\dot{W} - QU) \tag{9}$$

$$G_y = I_y\dot{Q} \tag{10}$$

2. Wheel Equations

The two degrees of freedom at the wheels give rise to two equations of motion: for heave and for pitch (Equations (6) and (7)). Again, the terms V,P, and R are zero, so these equations reduce to

$$F_{zi} = M_i(\dot{W}_i - Q_iU_i) \quad i = 1,2 \tag{11}$$

$$G_{yw} = I_{yw}\dot{Q}_w \tag{12}$$

where the subscripts denote front and rear wheels according to the notation of Figure 6, and

G_{yw} = the combined net torque on both wheels

I_{yw} = the combined wheel-drive train rotary moment of inertia

$Q_w = Q_1 = Q_2$ (since the wheels are not independent)

C. SOIL FORCES ON A RIGID WHEEL

In order to get expressions for the forces and moments in the equations of motion, I now turn to an analysis of the wheel-soil interaction.

All forces exerted on the wheel by the soil are assumed to arise from two basic stresses: normal stress and shear stress. The effects of these stresses are to resist sinkage and forward motion of the wheel due to compaction on the soil, to resist rotation of the wheel due to shearing of the soil, and to provide traction. Each stress will be considered individually, and examined for its effect on wheel motion. The rigid wheel case will be treated first, since it is applicable over a considerable range of sinkages for certain soils, and it is the simplest case to discuss.

1. Normal Stress Forces and Moments On a Rigid Wheel

The normal stress is directed radially inward on the wheel. A compressive stress is considered positive, no negative stresses are allowed, and the stress is assumed to be uniform across the width of the wheel. The stress at a given point is the average stress of an elemental force acting on an elemental area. Points on the wheel surface are located by an angle γ measured from the horizontal. A counterclockwise angle is positive. The angle to the point where the wheel first touches the soil (γ_1) is called the "entrance angle", and the angle to the point where the wheel leaves the soil (γ_2) is called the "exit angle." The area of soil-wheel contact between these two angles is called the "contact patch." Referring to Figure 7, the

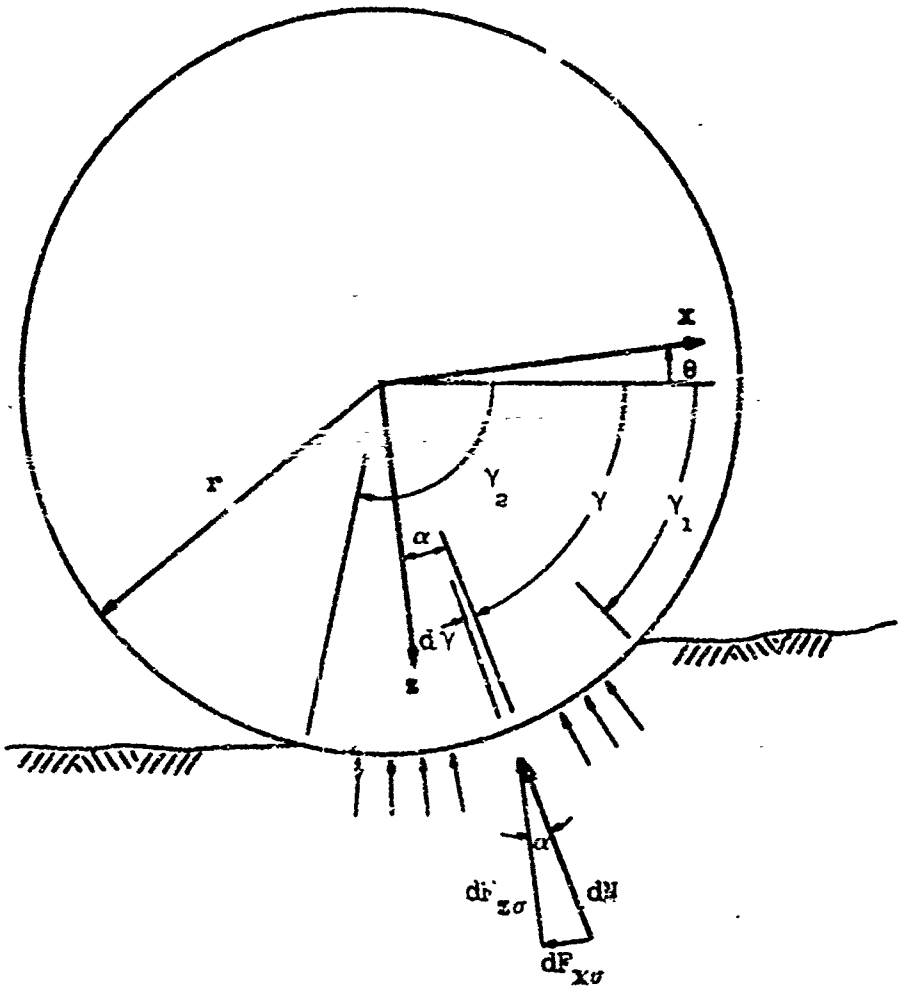

FIGURE 7 NORMAL STRESS UNDER A RIGID WHEEL

normal stress is expressed as

$$\sigma = \frac{dN}{b\ r\ d\gamma} \tag{13}$$

where b is the width of the wheel.

The normal stress produces forces which can be resolved into components in the vehicle coordinate system. This is shown in Figure 7. The component of the force on the wheel in the X direction due to normal stress is given as

$$dF_{x\sigma} = -\ dN \sin\alpha \tag{14}$$

Similiarly, the component of the force on the wheel in the Z direction due to normal stress is

$$dF_{z\sigma} = -\ dN \cos\alpha \tag{15}$$

From Figure 7

$$\alpha = \frac{\pi}{2} + \gamma - \theta = \frac{\pi}{2} + (\gamma - \theta) \tag{16}$$

From trigonometry

$$\sin\left[\frac{\pi}{2} + (\gamma - \theta)\right] = \cos(\gamma - \theta) \tag{17}$$

$$\cos\left[\frac{\pi}{2} + (\gamma - \theta)\right] = -\ \sin(\gamma - \theta) \tag{18}$$

From Equation (13)

$$dN = \sigma\ b\ r\ d\gamma \tag{19}$$

Substituting these into Equations (14) and (15) yields

$$dF_{x\sigma} = -\ b\ r\ \sigma \cos(\gamma - \theta) d\gamma \tag{20}$$

$$dF_{z\sigma} = b\ r\ \sigma \sin(\gamma - \theta) d\gamma \tag{21}$$

To get the total force on the wheel in each direction, Equations (20) and (21) are integrated across the entire contact patch, which is

located by the angles γ_1 and γ_2. Hence

$$F_{x\sigma} = -b\,r\int_{\gamma_2}^{\gamma_1} \sigma \cos(\gamma - \theta)d\gamma \tag{22}$$

$$F_{z\sigma} = b\,r\int_{\gamma_2}^{\gamma_1} \sigma \sin(\gamma - \theta)d\gamma \tag{23}$$

Since the normal stress acts radially, it produces no moment on the wheel. The forces due to normal stress do, however, produce a moment about the vehicle center of gravity. The component force in the Z direction is transmitted to the suspension, and is thereby accounted for in the equations of motion by the suspension forces. However, since there is no freedom in the X direction, the component force in the X direction is transmitted directly to the body. Designating the moment at the vehicle CG due to soil forces in the X direction as M_x, and referring to Figure 8,

$$dM_{x\sigma} = dF_{x\sigma}(Z_{Ri} + Z_i + r\cos\alpha) \tag{24}$$

where

Z_{Ri} = the "rest" position of the wheel

Z_i = the wheel displacement from the rest position

The sign of $dM_{x\sigma}$ will be determined by the sign of $dF_{x\sigma}$, since a positive $dF_{x\sigma}$ tends to rotate the vehicle in a positive direction, and a negative $dF_{x\sigma}$ tends to rotate the vehicle in a negative direction. The total moment follows by integration,

$$M_{x\sigma} = \int_{\gamma_2}^{\gamma_1} (Z_{Ri} + Z_i + r\cos\alpha)dF_{x\sigma} \tag{25}$$

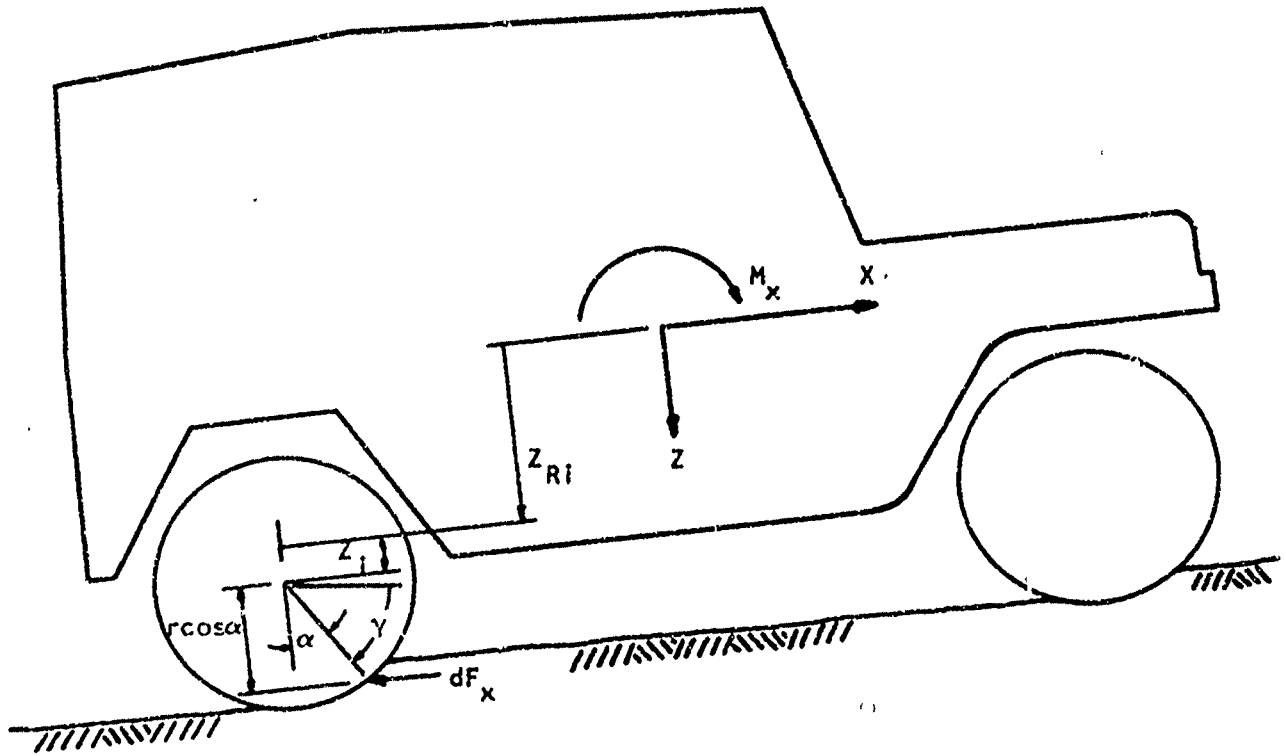

FIGURE 8 MOMENT AT VEHICLE CENTER OF GRAVITY DUE TO SOIL FORCES IN X-DIRECTION

$$M_{x\sigma} = (Z_{Ri} + Z_i)\int_{\gamma_2}^{\gamma_1} dF_{x\sigma} + \int_{\gamma_2}^{\gamma_1} r \cos\alpha \; dF_{x\sigma} \tag{26}$$

Substituting as before for $\cos\alpha$ and $dF_{x\sigma}$, and noting that $\int_{\gamma_2}^{\gamma_1} dF_{x\sigma} = F_{x\sigma}$, gives

$$M_{x\sigma} = (Z_{Ri} + Z_i)F_{x\sigma} + \; b\, r^2 \int_{\gamma_2}^{\gamma_1} \sigma \sin(\gamma - \theta)\cos(\gamma - \theta)\, d\gamma \tag{27}$$

Equations (22), (23), and (27) give the forces and moments which result from normal stresses on the wheel. Figure 7 shows that $F_{z\sigma}$ resists sinkage of the wheel, hence supports the vehicle, while $F_{x\sigma}$ resists forward motion of the wheel, hence resists forward motion of the vehicle.

2. Shear Stress Forces and Moments On a Rigid Wheel

The shear stress is directed tangentially on the wheel. A shear stress which resists the motion of a wheel associated with vehicle movement in the positive X direction is considered positive, and the stress is assumed to be uniform across the width of the wheel. Other assumptions and conventions for normal stress also hold. Referring to Figure 9, the shear stress is expressed as

$$\tau = \frac{dT}{b\, r\, d\gamma} \tag{28}$$

The shear stress produces forces which can be resolved into components in the vehicle coordinate system. This is shown in Figure 9. The component of the force on the wheel in the X direction due to shear stress is expressed as

$$dF_{x\tau} = dT \cos\alpha \tag{29}$$

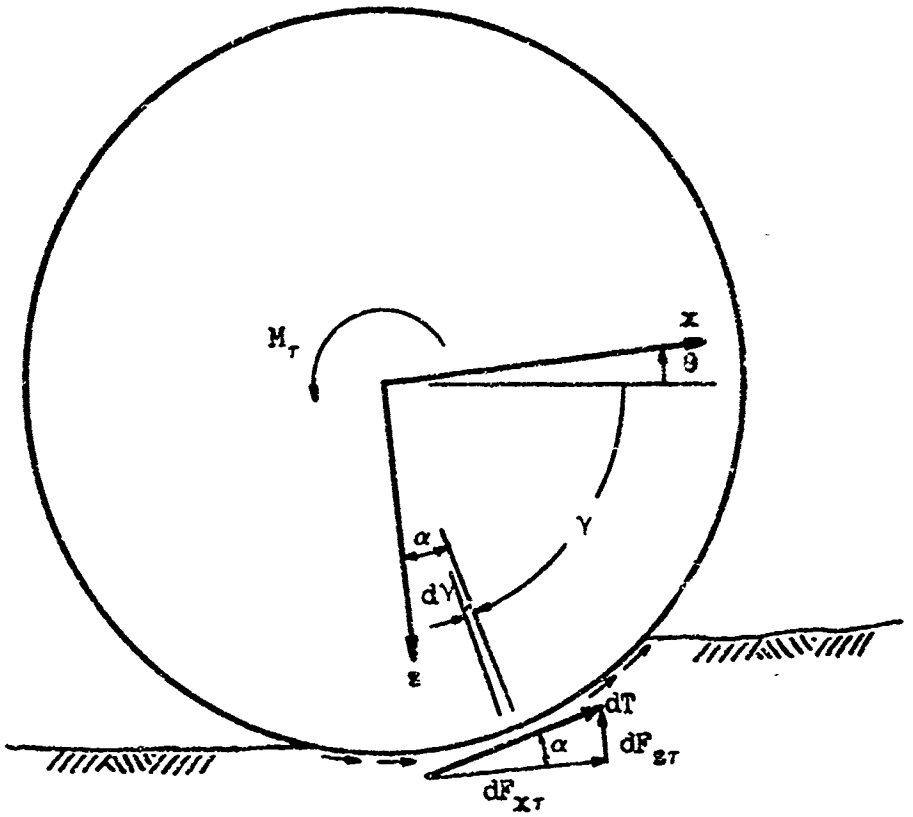

FIGURE 9 SHEAR STRESS UNDER A RIGID WHEEL

Similiarly, the component of the force on the wheel in the Z direction due to shear stress is

$$dF_{z\tau} = - dT \sin\alpha \tag{30}$$

From Equation (28)

$$dT = \tau\, b\, r\, d\gamma \tag{31}$$

Making this substitution, and the same substitution for α as before, Equations (29) and (30) become

$$dF_{x\tau} = - b\, r\, \tau \sin(\gamma - \theta) d\gamma \tag{32}$$

$$dF_{z\tau} = - b\, r\, \tau \cos(\gamma - \theta) d\gamma \tag{33}$$

Again, integration yields the total force on the wheel in each direction:

$$F_{x\tau} = - b\, r \int_{\gamma_2}^{\gamma_1} \tau \sin(\gamma - \theta) d\gamma \tag{34}$$

$$F_{z\tau} = - b\, r \int_{\gamma_2}^{\gamma_1} \tau \cos(\gamma - \theta) d\gamma \tag{35}$$

Since the shear stress acts tangentially, it tends to retard the rotation of the wheel. This can be measured as a moment at the wheel center. Designating this moment M_τ, and referring again to Figure 9,

$$dM_\tau = r\, dT \tag{36}$$

Making the previous substitution for dT, and integrating across the contact patch gives

$$M_\tau = b\, r^2 \int_{\gamma_2}^{\gamma_1} \tau\, d\gamma \tag{37}$$

As in the case of normal stress, the forces due to shear stress produce a moment about the vehicle center of gravity. Again, only the component force in the X direction is transmitted directly to the body.

The development of the expression for $M_{x\tau}$ is precisely the same as the development of $M_{x\sigma}$, with the obvious substitution of $dF_{x\tau}$ for $dF_{x\sigma}$. Hence,

$$M_{x\tau} = (Z_{Ri} + Z_i)F_{x\tau} + b\, r^2 \int_{\gamma_2}^{\gamma_1} \tau \sin(\gamma - \theta)\cos(\gamma - \theta)d\gamma \qquad (38)$$

Equations (34), (35), (37), and (38) give the forces and moments which result from shear stresses on the wheel. Figure 9 shows that $F_{z\tau}$ resists sinkage of the wheel, hence supports the vehicle, while $F_{x\tau}$ tends to move the wheel in the forward direction, hence provides traction.

D. NORMAL AND SHEAR STRESS FUNCTIONS

The task now is to express σ and τ as functions of γ. Numerous studies [12,13] have shown that normal stress is generally distributed in a symmetrical, bell-shaped, or sometimes parabolic, manner across the contact patch. However, no definitive formulation has yet been made. Therefore, the somewhat parabolic distribution shown in Figure 10 is assumed to be representative of the generally accepted theory. The equation for this distribution is

$$\sigma = \sigma_{max} \frac{(\gamma - \gamma_2)(\gamma - \gamma_1)}{(\gamma_{1/2} - \gamma_2)(\gamma_{1/2} - \gamma_1)} \qquad (39)$$

where

$$\gamma_{1/2} = \frac{\gamma_1 + \gamma_2}{2}$$

Expanding Equation (39) gives

$$\sigma = \frac{\sigma_{max}}{(\gamma_{1/2} - \gamma_2)(\gamma_{1/2} - \gamma_1)} \left[\gamma^2 - (\gamma_1 + \gamma_2)\gamma + \gamma_1 \gamma_2 \right] \qquad (40)$$

or, in simpler form,

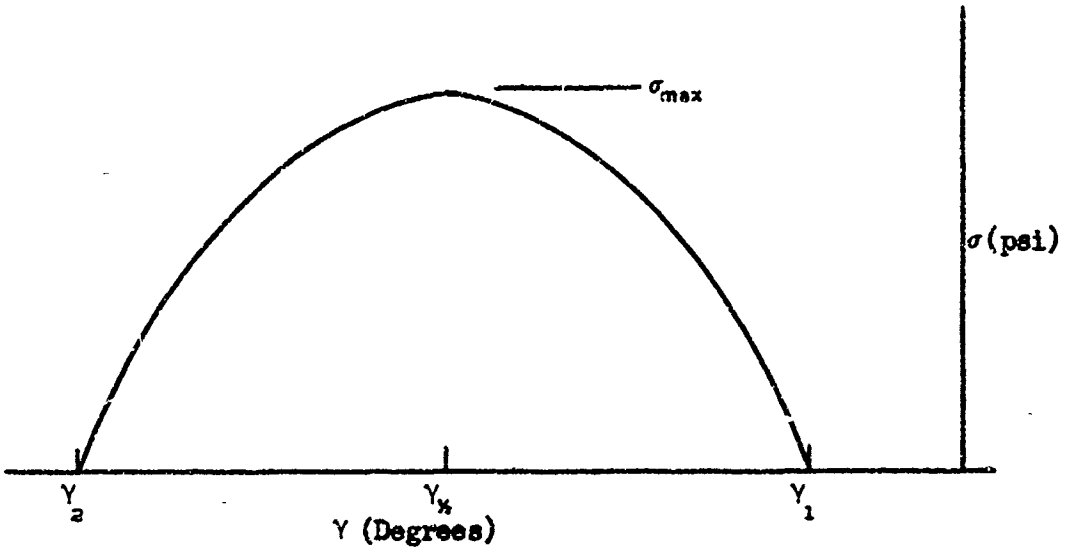

FIGURE 10 ASSUMED NORMAL STRESS DISTRIBUTION

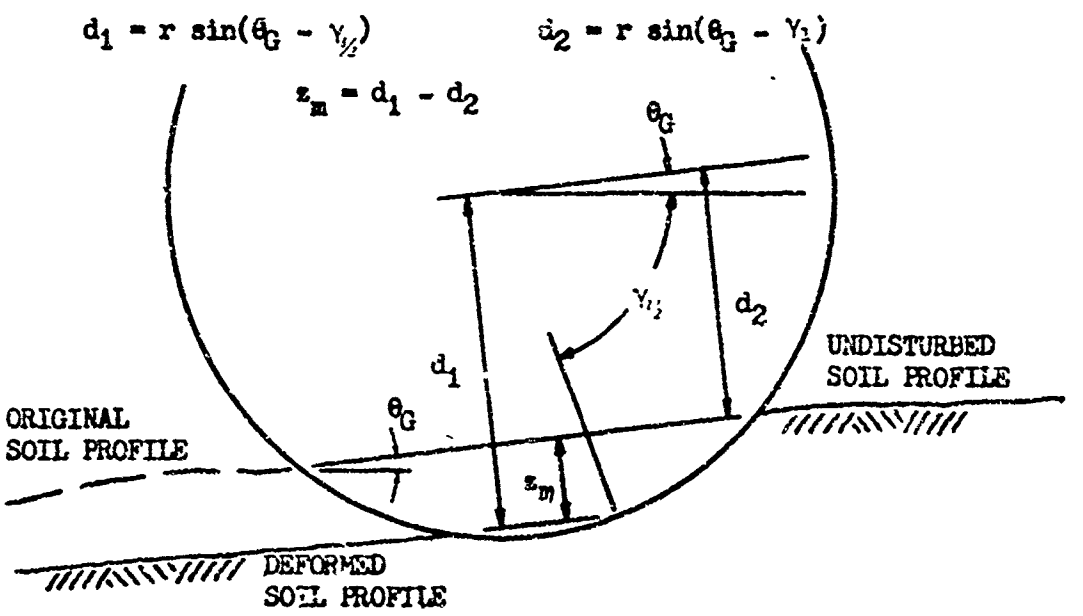

FIGURE 11 LOCAL GROUND SLOPE AND SINKAGE FOR A RIGID FRONT WHEEL

$$\sigma = A\gamma^2 + B\gamma + C \tag{41}$$

where

$$A = \frac{4\sigma_{max}}{(\gamma_1 - \gamma_2)(\gamma_2 - \gamma_1)}$$

$$B = -(\gamma_1 + \gamma_2)A$$

$$C = \gamma_1\gamma_2 A$$

The maximum normal stress, σ_{max}, occurs at the center of the contact patch. Bekker's equation for pressure, Equation (1), is used to determine σ_{max}. This requires an expression for the depth of sinkage at the center of the contact patch. Figure 11 shows a rigid wheel and a general soil profile. Since the soil is generally not exactly horizontal, or uniformly sloping, the angle θ_G is called the "local ground slope." It is the angle between the horizontal and the chord connecting the points of intersection of the wheel with the undisturbed soil profile at the front of the wheel, and the original soil profile at the rear of the wheel. All sinkages are measured perpendicular to this chord. The sinkage is given as

$$z_m = r\sin(\theta_G - \gamma_2) - r\sin(\theta_G - \gamma_1) \tag{42}$$

or

$$z_m = r\left[\sin(\theta_G - \gamma_2) - \sin(\theta_G - \gamma_1)\right] \tag{43}$$

The maximum pressure is now given as

$$\sigma_{max} = \left(\frac{k_c}{b} + k_\phi\right)z_m^n \tag{44}$$

Once the front wheels pass a point on the soil profile, the soil is compacted, and the rear wheels do not see the "original" soil profile. The normal stress distribution will now be modified to account

for this precompaction.

Figure 12 shows typical experimental pressure vs sinkage curves presented by Bekker [14]. These curves show how the pressure acts when the load on a plate is relieved, then re-applied. The curves show that when the load is re-applied, the pressure almost immediately returns to its value at the time the load was relieved from the plate. Soil engineers have used this behavior pattern for some time to aid in the construction of Void Ratio vs log Pressure curves used in studying consolidation settlements [8]. It is also the basis of the z_i term in the Sela-Ehrlich equation for pressure (Equation (2)). This pressure rebound is accounted for as shown in Figure 13. The normal stress distribution curve is assumed to be between the points located by the theoretical entrance angle with the original soil profile, called γ_{1o}, and the actual exit angle with the current, or existing, soil profile. The distribution curve is not extended to the theoretical exit angle with the original soil profile, γ_{2o}, since the pressure vs sinkage curves show that the pressure almost immediately drops to zero when the load is relieved. With these modifications, the factors in Equation (41) become, for the rear wheel,

$$A = \frac{4\sigma_{max}}{(\gamma_{1o} - \gamma_2)(\gamma_2 - \gamma_{1o})} \tag{45}$$

$$B = -(\gamma_{1o} + \gamma_2)A \tag{46}$$

$$C = \gamma_{1o}\gamma_2 A \tag{47}$$

The sinkage at the point of maximum stress, which is now at the center of the "modified" contact patch, is

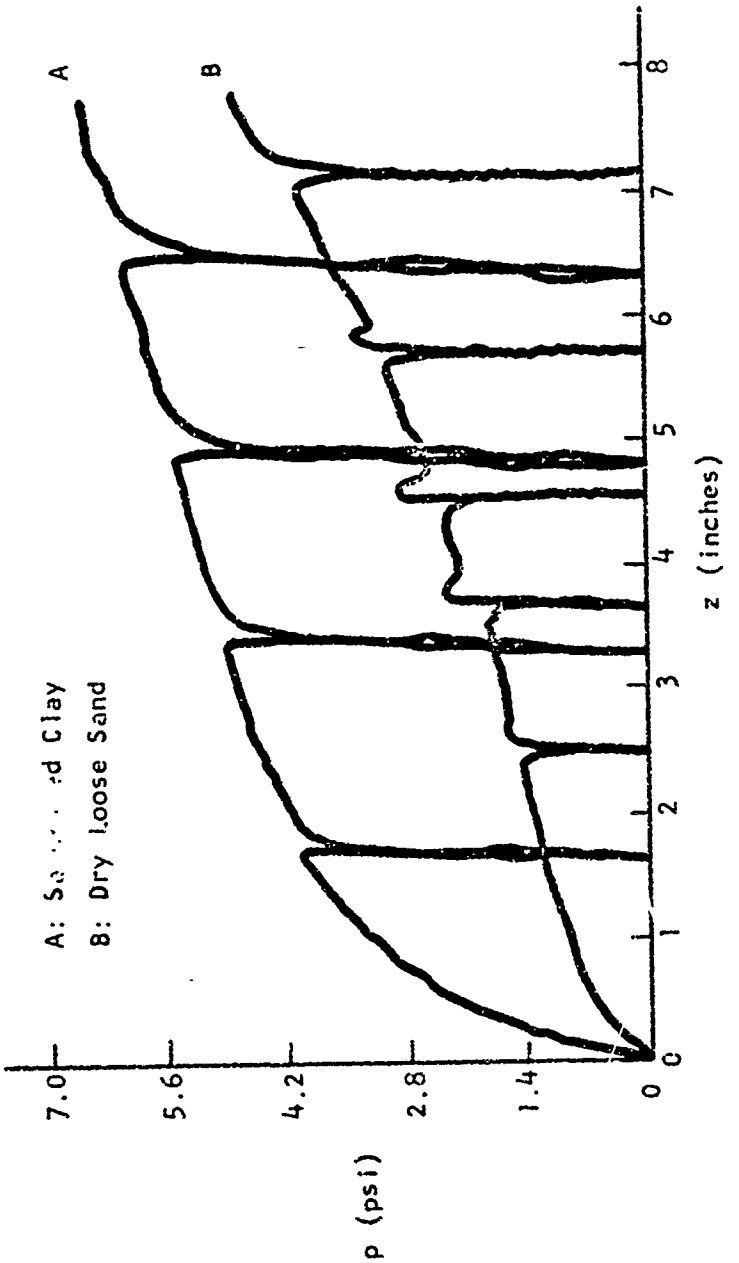

FIGURE 12 EXPERIMENTAL PRESSURE VS SINKAGE CURVES FROM REPETITIVE LOADING

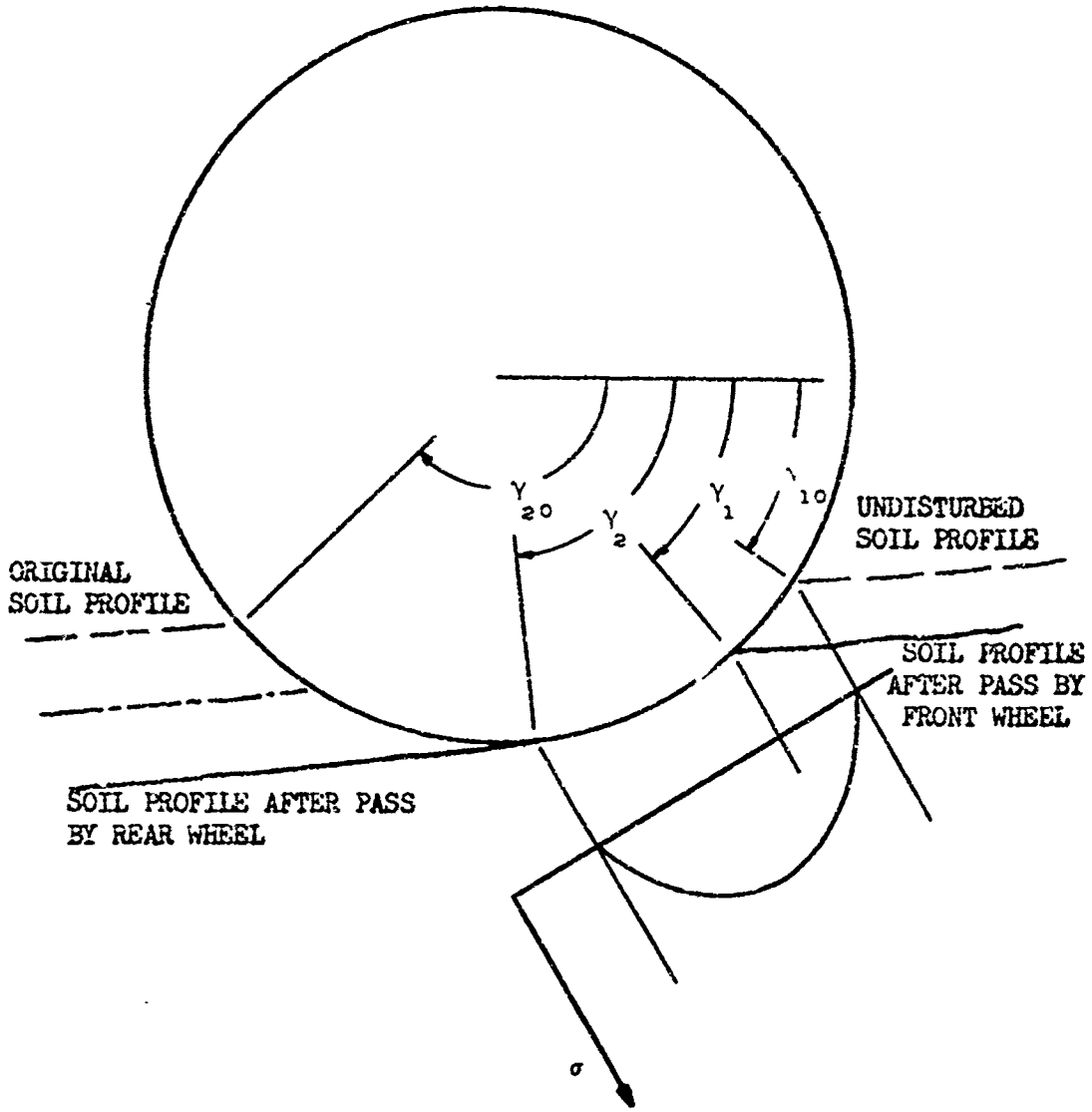

FIGURE 13 NORMAL STRESS DISTRIBUTION UNDER A REAR WHEEL

$$z_m = r\left[\sin\left(\theta_G - \frac{\gamma_{1o} + \gamma_2}{2}\right) - \sin(\theta_G - \gamma_{1o})\right] \tag{48}$$

For simplicity, Equations (45) - (48) will be used for both front and rear wheels, since for the front wheel, γ_{1o} is just equal to γ_1.

As noted in Section IIA, there exist several theories on the distribution of shear stress under a wheel undergoing slip. Janosi's approach is employed since it is generally used. Schuring and Belsdorf [1] presented an expression for j. As modified for the conventions and variables used in this report, the expression is

$$j = r\left[\gamma_1 - \gamma + (1 - s)\left(\cos(\gamma - \theta) - \cos(\gamma_1 - \theta)\right)\right] \tag{49}$$

where s is the wheel slip given by

$$s = \frac{r\dot{\theta}_W - \dot{X}}{r\dot{\theta}_W} \tag{50}$$

in which

r = the radius of the wheel

$\dot{\theta}_W$ = the angular velocity of the wheel

$\dot{X}$ = the velocity of the vehicle

Substitution of Equation (49) into Equation (4) gives the expression for shear stress:

$$\tau = (c + \sigma\tan\phi)\left\{1 - \exp\left(-\frac{r}{K}\left[\gamma_1 - \gamma + (1 - s)\left(\cos(\gamma - \theta) - \cos(\gamma_1 - \theta)\right)\right]\right)\right\} \tag{51}$$

E. INTEGRATION OF THE SOIL FORCE AND MOMENT EQUATIONS FOR THE RIGID WHEEL

1. Integrations Involving Normal Stress

Equation (41) makes it possible to integrate directly Equations (22), (23), and (27) for $F_{x\sigma}$, $F_{z\sigma}$, and $M_{x\sigma}$. With the substitution for σ, these equations become

$$F_{x\sigma} = -b\,r\int_{\gamma_2}^{\gamma_1}(A\gamma^2 + B\gamma + C)\cos(\gamma - \theta)\,d\gamma \tag{52}$$

$$F_{z\sigma} = b\,r\int_{\gamma_2}^{\gamma_1}(A\gamma^2 + B\gamma + C)\sin(\gamma - \theta)\,d\gamma \tag{53}$$

$$M_{x\sigma} = (Z_{Ri} + Z_i)F_{x\sigma} + b\,r^2\int_{\gamma_2}^{\gamma_1}(A\gamma^2 + B\gamma + C)\sin(\gamma - \theta)\cos(\gamma - \theta)\,d\gamma \tag{54}$$

These are involved, but straightforward problems in integration by parts. The results are:

$$F_{x\sigma} = b\,r\Big\{-(A\gamma_1^2 + B\gamma_1 + C)\sin(\gamma_1 - \theta) + A\Big[(\gamma_2 - \gamma_{1c})\cos(\gamma_2 - \theta) + (\gamma_2 - 2\gamma_1 + \gamma_{1c})\cos(\gamma_1 - \theta) + 2\big(\sin(\gamma_1 - \theta) - \sin(\gamma_2 - \theta)\big)\Big]\Big\} \tag{55}$$

$$F_{z\sigma} = b\,r\Big\{-(A\gamma_1^2 + B\gamma_1 + C)\cos(\gamma_1 - \theta) + A\Big[(\gamma_{10} - \gamma_2)\sin(\gamma_2 - \theta) + (2\gamma_1 - \gamma_{10} - \gamma_2)\sin(\gamma_1 - \theta) + 2\big(\cos(\gamma_1 - \theta) - \cos(\gamma_2 - \theta)\big)\Big]\Big\} \tag{56}$$

$$M_{x\sigma} = (Z_{Ri} + Z_i)F_{x\sigma} + b\,r^2 \Big\{ (A\gamma_1^2 + B\gamma_1 + C)\tfrac{1}{2}\sin^2(\gamma_1 - \theta) +$$

$$\frac{A}{8}\Big[2(\gamma_{10} - \gamma_1)(\gamma_1 - \gamma_2) + (\gamma_{10} - \gamma_2)\sin\big(2(\gamma_2 - \theta)\big) +$$

$$(2\gamma_1 - \gamma_{10} + \gamma_2)\sin\big(2(\gamma_1 - \theta)\big) + \cos\big(2(\gamma_1 - \theta)\big) -$$

$$\cos\big(2(\gamma_2 - \theta)\big)\Big]\Big\} \qquad (57)$$

When evaluated for a given wheel position, Equations (55) and (57) are inserted into the hull equations of motion, while Equation (56) is inserted into the wheel equations of motion as shown below.

2. Integrations Involving Shear Stress

Equation (51) makes it extremely difficult to integrate directly Equations (34), (35), (37), and (38) for F_{xr}, F_{zr}, M_r, and M_{xr}. A numerical integration simplifies the problem considerably, and is easily implemented on a computer. An accurate method is the Newton-Cotes 5-Point Method. As an illustration, the integral of the shear stress equation was calculated by two methods for various values of γ_1 and γ_2. One method was the Newton-Cotes Method, the other was the Trapezoid Method, using intervals of five degrees. The Trapezoid Method is known to be an accurate numerical method for computing integrals, but it requires many more computations than the Newton-Cotes Method. The results are shown in Table 1. In all cases, the value computed by the Newton-Cotes Method was within 0.48% of the value

TABLE 1

COMPARISON OF NUMERICAL INTEGRATION METHODS

SLIP	γ_1	γ_2	AREA BY NEWTON-COTES	AREA BY TRAPEZOID	DEVIATION
0%	-20°	-110°	4.461263	4.481281	0.45%
0%	-30°	-110°	2.516806	2.529037	0.48%
0%	-40°	-110°	1.156235	1.161734	0.47%
20%	-20°	-110°	5.170466	5.187438	0.33%
20%	-30°	-110°	3.327870	3.337837	0.30%
20%	-40°	-110°	1.890615	1.894482	0.20%
40%	-20°	-110°	5.543898	5.562296	0.33%
40%	-30°	-110°	3.759944	3.771866	0.32%
40%	-40°	-110°	2.294688	2.300244	0.24%
60%	-20°	-110°	5.757924	5.777705	0.34%
60%	-30°	-110°	4.007252	4.021091	0.34%
60%	-40°	-110°	2.530277	2.527608	0.29%
80%	-20°	-110°	5.890605	5.910926	0.34%
80%	-30°	-110°	4.158725	4.173727	0.36%
80%	-40°	-110°	2.675515	2.684094	0.32%
100%	-20°	-110°	5.978328	5.998789	0.34%
100%	-30°	-110°	4.257007	4.272829	0.37%
100%	-40°	-110°	2.769586	2.779135	0.34%

computed by the Trapezoid Method. When evaluated, these force and moment terms are inserted into the equations of motion in a manner similiar to that for normal stress.

F. SOIL FORCES ON A FLEXIBLE WHEEL

1. Tire Deflection

As long as the pressure exerted on a tire by a soil stays below some maximum value, the tire acts like a rigid wheel. When the soil pressure reaches this maximum value, the tire deflects. The maximum allowable value of soil pressure under a wheel is assumed to be expressible as

$$P' = P_i + P_c \tag{58}$$

where

P' = the maximum soil pressure

P_i = the inflation pressure within the tire

P_c = the carcass pressure of the tire

This assumption, and the assumption of a symmetrical normal stress distribution with maximum value at the centerline of the modified contact patch (Section III.D) leads to the following analysis:

a. The first deflection of the tire will be at the centerline of the modified contact patch if the maximum soil pressure reaches P'.

b. Since the soil pressure cannot exceed P', the normal pressure distribution may be based upon a theoretical sinkage which would obtain if the wheel remained rigid. This theoretical sinkage is called z_{mTH}, and the corresponding theoretical maximum normal stress is called σ_{maxTH}.

c. As σ_{maxTH} increases, more of the tire deflects. The "zone of tire deflection" is defined by that portion of the theoretical normal pressure distribution which has ordinates greater than P'. Note that the zone of tire deflection is symmetrical about the centerline of the modified contact patch, and that the normal pressure in the zone is P'.

Additionally, the tire deflection is assumed to be linear. A typically deflected tire and its associated normal stress distribution as assumed in this report is shown in Figure 14.

Justification for this assumed stress distribution has been presented by Ellis [15], who shows that the pressure under a flexible tire on a hard surface is nearly uniform across the contact patch, and drops off sharply at the leading and trailing edges. Since the soil pressure is at the maximum allowable under the deflected portion of the tire, the soil will not deflect any further, hence it acts as a rigid surface. The remainder of the tire still in contact with the soil will behave according to the rigid wheel theory described above.

The problem of integrating Equations (22), (23), and (27) is altered only by the need to know two additional angles (γ_{1P} and γ_{2P}) for limits of integration. For the flexible wheel case, Equation (22), for example, becomes

$$F_{x\sigma} = -b\,r\int_{\gamma_2}^{\gamma_{2P}} \sigma \cos(\gamma - \theta)\, d\gamma - b\,r\,P'\int_{\gamma_{2P}}^{\gamma_{1P}} \cos(\gamma - \theta)\, d\gamma - b\,r\int_{\gamma_{1P}}^{\gamma_1} \sigma \cos(\gamma - \theta)\, d\gamma \qquad (59)$$

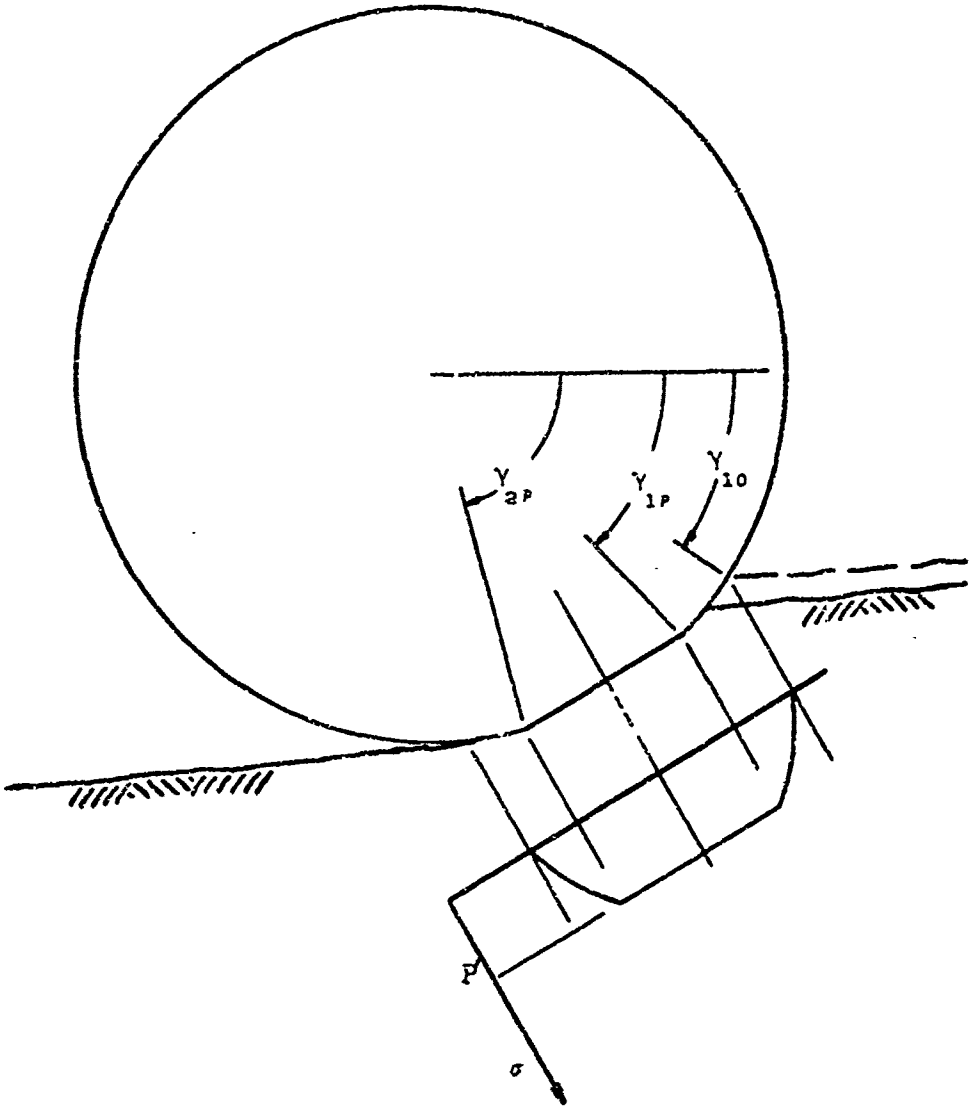

FIGURE 14 NORMAL STRESS DISTRIBUTION UNDER A FLEXIBLE WHEEL

Consider the equation for normal stress distribution,

$$\sigma = A\gamma^2 + B\gamma + C \tag{60}$$

It is necessary to solve this for the angles when $\sigma = P'$. Note that in the expression for A, $\sigma_{max} = \sigma_{maxTH}$. Substituting for σ in Equation (60) gives

$$A\gamma^2 + B\gamma + C = P' \tag{61}$$

or

$$A\gamma^2 + B\gamma + (C - P') = 0 \tag{62}$$

Applying the quadratic formula to solve for γ gives

$$\gamma = \frac{-B \pm \sqrt{B^2 - 4A(C - P')}}{2A} \tag{63}$$

Making the appropriate substitutions for A, B, and C, and then simplifying yields

$$\gamma = \tfrac{1}{2}(\gamma_{10} + \gamma_2) \pm \tfrac{1}{2}(\gamma_{10} - \gamma_2)\sqrt{1 - \frac{P'}{\sigma_{maxTH}}} \tag{64}$$

From this, the limits of the tire deflection area are

$$\gamma_{1P} = \tfrac{1}{2}\left\{\gamma_{10} + \gamma_2 + (\gamma_{10} - \gamma_2)\sqrt{1 - \frac{P'}{\sigma_{maxTH}}}\right\} \tag{65}$$

$$\gamma_{2P} = \tfrac{1}{2}\left\{\gamma_{10} + \gamma_2 - (\gamma_{10} - \gamma_2)\sqrt{1 - \frac{P'}{\sigma_{maxTH}}}\right\} \tag{66}$$

2. Normal Stress Forces and Moments On a Flexible Wheel

Figure 15 shows the normal stresses acting on a deflected tire. Note that in the zone of tire deflection, the stress no longer acts radially, since it is perpendicular to the deflected portion of the tire. This means that at any point along the deflection zone, the same angle is used to resolve the forces due to normal stress into

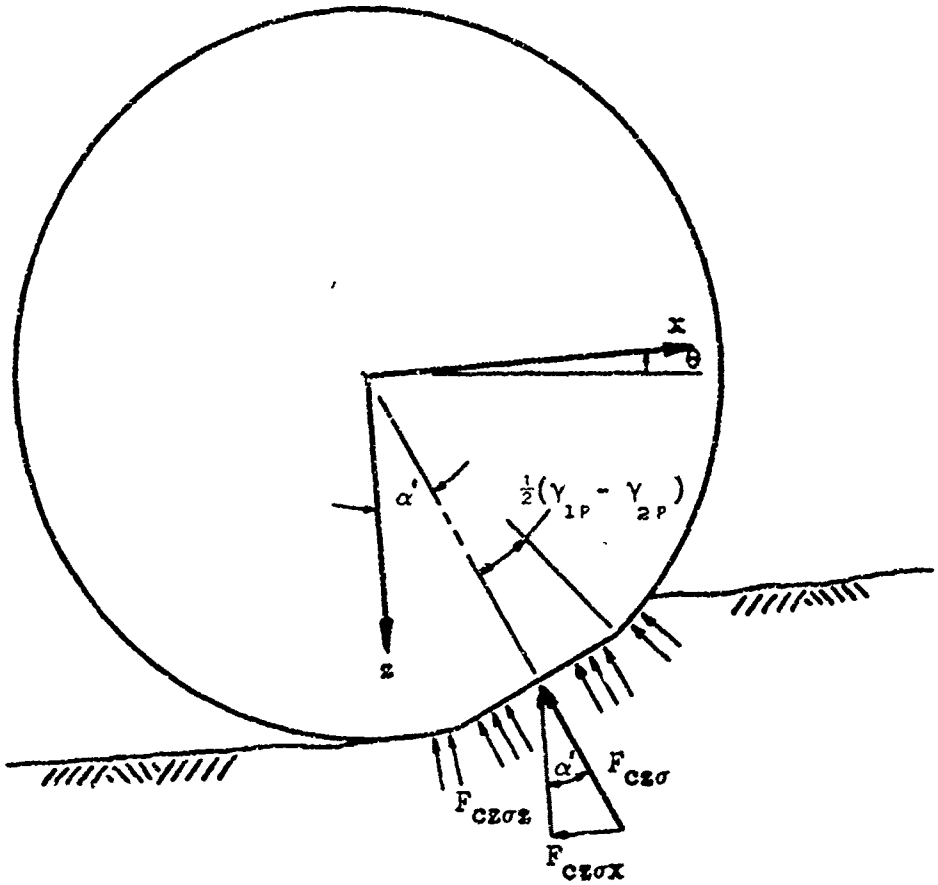

FIGURE 15 NORMAL STRESS UNDER A FLEXIBLE WHEEL

components in the vehicle coordinate system. This angle is the angle between the centerline of the deflection zone, and the Z axis. From Figure 15, the angle is

$$\alpha' = \tfrac{1}{2}\pi + \tfrac{1}{2}(\gamma_{10} + \gamma_2) - \theta \tag{67}$$

Note also that the expression for dN (Equation (19)) is no longer valid since the incremental area is no longer equal to b r $d\gamma$. However, it is not necessary to integrate actually any functions in the zone of deflection. Because of the symmetry and constant pressure in the zone of deflection, the resultant of all stresses in the zone acts at the centerline of the modified contact patch. To find the resultant, consider the contact patch in the zone of deflection. Since it is the chord of a circle, the length of the patch is given by

$$L = 2\ r\ \sin\left(\tfrac{1}{2}(\gamma_{1P} - \gamma_{2P})\right) \tag{68}$$

The resultant is then

$$F_{cz\sigma} = 2\ b\ r\ P'\sin\left(\tfrac{1}{2}(\gamma_{1P} - \gamma_{2P})\right) \tag{69}$$

The components of the resultant force in the X and Z directions are:

$$F_{cz\sigma x} = -\ 2\ b\ r\ P'\sin\left(\tfrac{1}{2}(\gamma_{1P} - \gamma_{2P})\right)\sin\alpha'$$

$$= -\ 2\ b\ r\ P'\sin\left(\tfrac{1}{2}(\gamma_{1P} - \gamma_{2P})\right)\cos\left(\tfrac{1}{2}(\gamma_{10} + \gamma_2) - \theta\right) \tag{70}$$

$$F_{cz\sigma z} = -\ 2\ b\ r\ P'\sin\left(\tfrac{1}{2}(\gamma_{1P} - \gamma_{2P})\right)\cos\alpha'$$

$$= 2\ b\ r\ P'\sin\left(\tfrac{1}{2}(\gamma_{1P} - \gamma_{2P})\right)\sin\left(\tfrac{1}{2}(\gamma_{10} + \gamma_2) - \theta\right) \tag{71}$$

Equations (22) and (23) can now be modified for the flexible wheel:

$$F_{x\sigma} = -b\,r\int_{\gamma_2}^{\gamma_{2P}} \sigma\cos(\gamma - \theta)\,d\gamma - b\,r\int_{\gamma_{1P}}^{\gamma_1} \sigma\cos(\gamma - \theta)\,d\gamma$$

$$- 2\,b\,r\,P'\sin\left(\tfrac{1}{2}(\gamma_{1P} - \gamma_{2P})\right)\cos\left(\tfrac{1}{2}(\gamma_{10} + \gamma_2) - \theta\right) \tag{72}$$

$$F_{z\sigma} = b\,r\int_{\gamma_2}^{\gamma_{2P}} \sigma\sin(\gamma - \theta)\,d\gamma + b\,r\int_{\gamma_{1P}}^{\gamma_1} \sigma\sin(\gamma - \theta)\,d\gamma$$

$$+ 2\,b\,r\,P'\sin\left(\tfrac{1}{2}(\gamma_{1P} - \gamma_{2P})\right)\sin\left(\tfrac{1}{2}(\gamma_{10} + \gamma_2) - \theta\right) \tag{73}$$

Even though the stress in the zone of deflection no longer acts radially, it still does not produce a moment on the wheel because it is symmetrical about the centerline of the contact patch. However, the moment about the vehicle CG due to the components of forces due to normal stress is affected, because the moment arm is no longer measured from the edge of a circle, as it was for the rigid wheel.

Since the resultant $F_{cz\sigma}$ acts at the center of the contact zone, the moment arm from its X component to the x axis of the wheel is

$$d = r\cos\left(\tfrac{1}{2}(\gamma_{1P} - \gamma_{2P})\right)\cos(\alpha') \tag{74}$$

The moment about the vehicle CG due to the X component of $F_{cz\sigma}$ is

$$M' = F_{cz\sigma x}(Z_{Ri} + Z_i + d) \tag{75}$$

$$M' = -2\,b\,r\,P'\sin\tfrac{1}{2}(\gamma_{1P} - \gamma_{2P})\cos\left(\tfrac{1}{2}(\gamma_{10} + \gamma_2) - \theta\right)\Big[Z_{Ri} +$$

$$Z_i - r\cos\tfrac{1}{2}(\gamma_{1P} - \gamma_{2P})\sin\left(\tfrac{1}{2}(\gamma_{10} + \gamma_2) - \theta\right)\Big] \tag{76}$$

Finally, the expression for $M_{x\sigma}$ follows from Equation (24)

$$M_{x\sigma} = \int_{\gamma_2}^{\gamma_{2P}} (Z_{Ri} + Z_i + r\cos\alpha)\,dF_{x\sigma} + M' + \int_{\gamma_{1P}}^{\gamma_1} (Z_{Ri} + Z_i + r\cos\alpha)\,dF_{x\sigma} \tag{77}$$

In order to be able to write this in a somewhat condensed form, let

$$\gamma_{\frac{1}{2}P} = \tfrac{1}{2}(\gamma_{1P} - \gamma_{2P}) \tag{78}$$

$$\beta = \tfrac{1}{2}(\gamma_{10} + \gamma_{2}) - \theta \tag{79}$$

Then

$$M_{x\sigma} = b\,r\,(Z_{Ri} + Z_i)\left[-\int_{\gamma_2}^{\gamma_{2P}} \sigma\cos(\gamma - \theta)\,d\gamma - \int_{\gamma_{1P}}^{\gamma_1} \sigma\cos(\gamma - \theta)\,d\gamma\right] -$$

$$2\,b\,r\,P'\sin(\gamma_{\frac{1}{2}P})\cos(\beta)\left[Z_{Ri} + Z_i - r\cos(\gamma_{\frac{1}{2}P})\sin(\beta)\right] +$$

$$b\,r^2\left[\int_{\gamma_2}^{\gamma_{2P}} \sigma\sin(\gamma - \theta)\cos(\gamma -)\,d\gamma + \int_{\gamma_{1P}}^{\gamma_1} \sigma\sin(\gamma - \theta)\cos(\gamma - \theta)d\gamma\right] \tag{80}$$

Equations (72), (73), and (80) give the forces and moments which result from normal stresses on a flexible wheel.

3. Shear Stress Forces and Moments On a Flexible Wheel

Figure 16 shows the shear stresses acting on a deflected tire. As in the case of normal stress, at any point along the deflection zone, the same angle is used to resolve the forces due to shear stress into components in the vehicle coordinate system. The approach to finding the resultant of the shear stresses acting in the deflection zone is the same one used for normal stress. It does, however, require the simplifying assumption that while the shear stress distribution is not symmetrical about the centerline of the contact patch, the eccentricity is small enough to neglect.

Figure 17 shows a typical shear stress distribution under a deflected tire as calculated from Equation (51), using $\sigma = P'$ in the zone of deflection. Note that it is not symmetrical about the centerline of the contact patch. The centroid of the area bounded by γ_{1P} and γ_{2P}

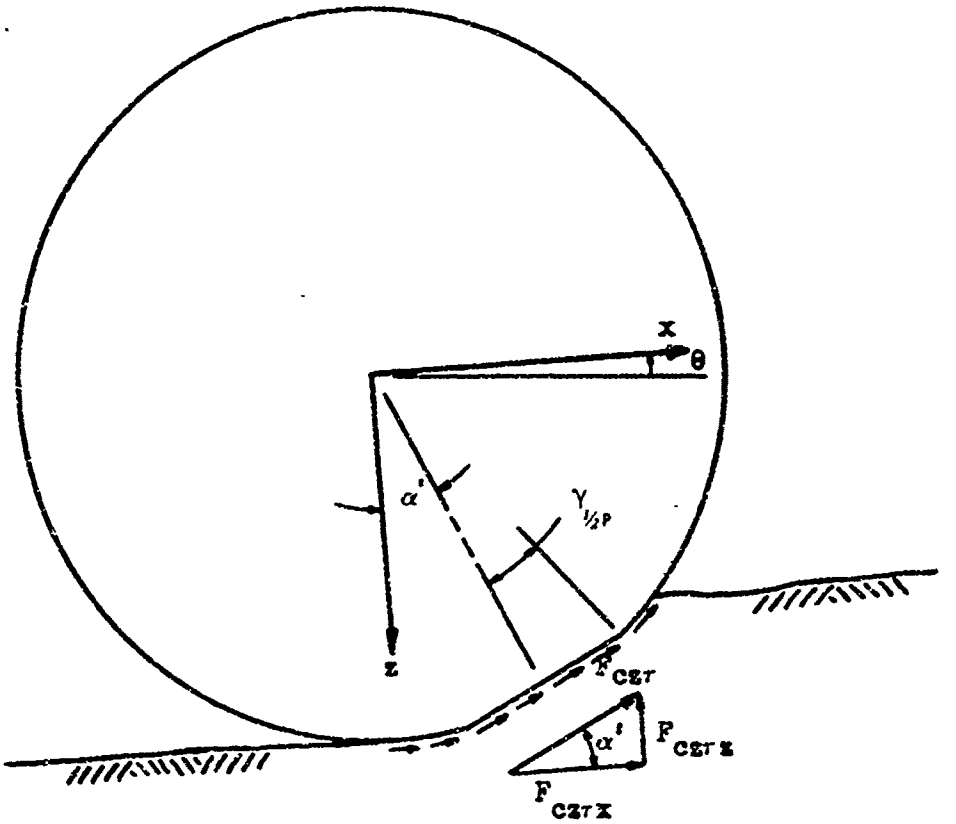

FIGURE 16 SHEAR STRESS UNDER A FLEXIBLE WHEEL

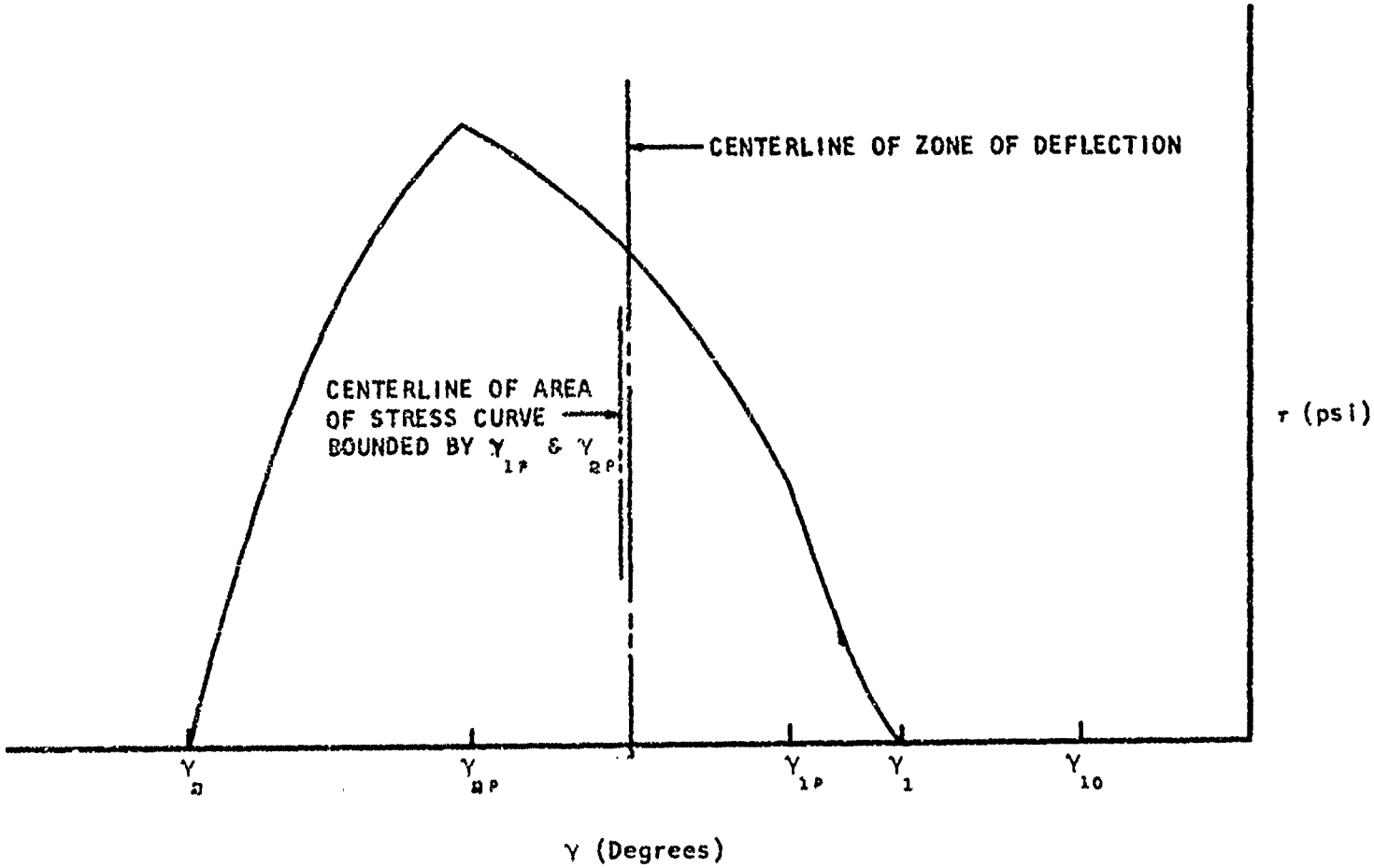

FIGURE 17 SHEAR STRESS DISTRIBUTION UNDER A DEFLECTED TIRE

(and hence, the point of action of the resultant), does not lie on the centerline of the zone of deflection. The eccentricity in terms of is approximately 1°. This eccentricity affects two values: the moment arm of $F_{cz\tau}$ about the wheel center, and the moment arm from $F_{cz\tau x}$ to the x axis of the wheel. Both of these values are affected because of the term $r \cos(\gamma_{1/2p})$. For values of $\gamma_{1/2p}$ which can reasonably be expected ($\gamma_{1/2p} \leq 20^{\circ}$), the difference between $r \cos(\gamma_{1/2p})$ and $r \cos(\gamma_{1/2p} + 1^{\circ})$ is negligible.

The resultant of the forces due to shear stress in the zone of deflection can now be written as

$$F_{cz\tau} = 2\, b\, r \sin(\gamma_{1/2p}) \int_{\gamma_{2p}}^{\gamma_{1p}} \tau \, d\gamma \tag{81}$$

The components of the resultant force in the X and Z directions are:

$$F_{cz\tau x} = 2\, b\, r \sin(\gamma_{1/2p}) \cos\alpha' \int_{\gamma_{2p}}^{\gamma_{1p}} \tau \, d\gamma$$

$$= -2\, b\, r \sin(\gamma_{1/2p}) \sin(\beta) \int_{\gamma_{2p}}^{\gamma_{1p}} \tau \, d\gamma \tag{82}$$

$$F_{cz\tau z} = -2\, b\, r \sin(\gamma_{1/2p}) \sin\alpha' \int_{\gamma_{2p}}^{\gamma_{1p}} \tau \, d\gamma$$

$$= -2\, b\, r \sin(\gamma_{1/2p}) \cos(\beta) \int_{\gamma_{2p}}^{\gamma_{1p}} \tau \, d\gamma \tag{83}$$

Equations (34) and (35) can now be modified for the flexible wheel:

$$F_{x\tau} = -b\, r \int_{\gamma_2}^{\gamma_{2p}} \tau \sin(\gamma - \theta)\, d\gamma - b\, r \int_{\gamma_{1p}}^{\gamma_1} \tau \sin(\gamma - \theta)\, d\gamma$$

$$- 2\, b\, r \sin(\gamma_{1/2p}) \sin(\beta) \int_{\gamma_{2p}}^{\gamma_{1p}} \tau \, d\gamma \tag{84}$$

$$F_{z\tau} = -b\,r\int_{\gamma_2}^{\gamma_{2P}} \tau\cos(\gamma-\theta)\,d\gamma - b\,r\int_{\gamma_{1P}}^{\gamma_1} \tau\cos(\gamma-\theta)\,d\gamma$$

$$-2\,b\,r\,\sin(\gamma_{\frac{1}{2}P})\,\cos(\beta)\int_{\gamma_{2P}}^{\gamma_{1P}} \tau\,d\gamma \tag{85}$$

The expression for the moment on the wheel of forces due to shear stress, Equation (37), is easily modified for the flexible wheel by using the resultant $F_{cz\tau}$ and its moment arm, $r\cos(\gamma_{\frac{1}{2}P})$.

$$M_\tau = b\,r^2\int_{\gamma_2}^{\gamma_{2P}} \tau\,d\gamma + 2\,b\,r^2\,\sin(\gamma_{\frac{1}{2}P})\,\cos(\gamma_{\frac{1}{2}P})\int_{\gamma_{2P}}^{\gamma_{1P}} \tau\,d\gamma + b\,r^2\int_{\gamma_{1P}}^{\gamma_1} \tau\,d\gamma \tag{86}$$

The moment about the vehicle CG due to the X component of $F_{cz\tau}$ is

$$M'' = F_{cz\tau x}(Z_{Ri} + Z_i + d) \tag{87}$$

$$M'' = -2\,b\,r\,\sin(\gamma_{\frac{1}{2}P})\,\sin(\beta)\Big[Z_{Ri} + Z_i +$$

$$r\cos(\gamma_{\frac{1}{2}P})\,\sin(\beta)\Big]\int_{\gamma_{2P}}^{\gamma_{1P}} \tau\,d\gamma \tag{88}$$

Then the expression for $M_{x\tau}$ follows from Equation (24):

$$M_{x\tau} = \int_{\gamma_2}^{\gamma_{2P}} (Z_{Ri} + Z_i + r\cos\alpha)\,dF_{x\tau} + M'' + \int_{\gamma_{1P}}^{\gamma_1} (Z_{Ri} + Z_i + r\cos\alpha)\,dF_{x\tau} \tag{89}$$

$$M_{x\tau} = b\,r\,(Z_{Ri} + Z_i)\left[-\int_{\gamma_2}^{\gamma_{2P}} \tau\sin(\gamma-\theta)\,d\gamma - \int_{\gamma_{1P}}^{\gamma_1} \tau\sin(\gamma-\theta)\,d\gamma\right] -$$

$$2\,b\,r\,\sin(\gamma_{\frac{1}{2}P})\,\sin(\beta)\left(Z_{Ri} + Z_i - r\cos(\gamma_{\frac{1}{2}P})\,\sin(\beta)\right)\int_{\gamma_{2P}}^{\gamma_{1P}} \tau\,d\gamma +$$

$$b\,r^2\left[\int_{\gamma_2}^{\gamma_{2P}} \tau\sin^2(\gamma-\theta)\,d\gamma + \int_{\gamma_{1P}}^{\gamma_1} \tau\sin^2(\gamma-\theta)\,d\gamma\right] \tag{90}$$

Equations (84), (85), (86), and (90) give the forces and moments which result from shear stresses on a flexible wheel.

G. INTEGRATION OF THE SOIL FORCE AND MOMENT EQUATIONS FOR THE FLEXIBLE WHEEL

1. Integrations Involving Normal Stress

As in the rigid wheel case, the expressions for $F_{x\sigma}$, $F_{z\sigma}$, and $M_{x\sigma}$ are analytically integrable. The results of the integrations from the rigid wheel case are directly applicable to the flexible wheel case, since the only difference is the limits of integration. The results are:

$$
\begin{aligned}
F_{x\sigma} = b\,r\Big\{&(A\gamma_{1P}^2 + B\gamma_{1P} + C)\sin(\gamma_{1P} - \theta) - (A\gamma_1^2 + B\gamma_1 + C)\sin(\gamma_1 - \theta) \\
&- (A\gamma_{2P}^2 + B\gamma_{2P} + C)\sin(\gamma_{2P} - \theta) + A\Big[(\gamma_2 - \gamma_{10})\cos(\gamma_2 - \theta) \\
&+ (\gamma_2 - 2\gamma_{2P} + \gamma_{10})\cos(\gamma_{2P} - \theta) + 2\big(\sin(\gamma_{2P} - \theta) - \sin(\gamma_2 - \theta)\big) \\
&+ (\gamma_{1P} - \gamma_{10})\cos(\gamma_{1P} - \theta) + (\gamma_{1P} - 2\gamma_1 + \gamma_{10})\cos(\gamma_1 - \theta) \\
&+ 2\big(\sin(\gamma_1 - \theta) - \sin(\gamma_{1P} - \theta)\big)\Big] - 2\,P'\sin(\gamma_{1/2P})\cos(\beta)\Big\}
\end{aligned}
\tag{91}
$$

$$
\begin{aligned}
F_{z\sigma} = b\,r\Big\{&(A\gamma_{1P}^2 + B\gamma_{1P} + C)\cos(\gamma_{1P} - \theta) - (A\gamma_1^2 + B\gamma_1 + C)\cos(\gamma_1 - \theta) \\
&- (A\gamma_{2P}^2 + B\gamma_{2P} + C)\cos(\gamma_{2P} - \theta) + A\Big[(\gamma_{10} - \gamma_2)\cos(\gamma_2 - \theta) \\
&+ (2\gamma_{2P} - \gamma_2 - \gamma_{10})\sin(\gamma_{2P} - \theta) + 2\big(\cos(\gamma_{2P} - \theta) - \cos(\gamma_2 - \theta)\big) \\
&+ (\gamma_{10} - \gamma_{1P})\sin(\gamma_{1P} - \theta) + (2\gamma_1 - \gamma_{10} - \gamma_{1P})\sin(\gamma_1 - \theta) \\
&+ 2\big(\cos(\gamma_1 - \theta) - \cos(\gamma_{1P} - \theta)\big)\Big] + 2\,P'\sin(\gamma_{1/2P})\sin(\beta)\Big\}
\end{aligned}
\tag{92}
$$

$$
\begin{aligned}
M_{x\sigma} = {} & (Z_{Ri} + Z_i)F_{x\sigma} + 2\,b\,r^2\,P'\sin(\gamma_{\frac{1}{2}P})\cos(\gamma_{\frac{1}{2}P})\sin(\beta)\cos(\beta) \\
& + b\,r^2\Big\{(A\gamma_{2P}^2 + B\gamma_{2P} + C)\tfrac{1}{2}\sin^2(\gamma_{2P} - \theta) \\
& + (A\gamma_1^2 + B\gamma_1 + C)\tfrac{1}{2}\sin^2(\gamma_1 - \theta) - (A\gamma_{1P}^2 + B\gamma_{1P} + C)\tfrac{1}{2}\sin^2(\gamma_{1P} - \theta) \\
& + \frac{A}{8}\Big[2(\gamma_{10} - \gamma_{2P})(\gamma_{2P} - \gamma_2) + (\gamma_{10} - \gamma_2)\sin\big(2(\gamma_2 - \theta)\big) \\
& + (2\gamma_{2P} - \gamma_{10} + \gamma_2)\sin\big(2(\gamma_{2P} - \theta)\big) + \cos\big(2(\gamma_{2P} - \theta)\big) - \cos\big(2(\gamma_2 - \theta)\big) \\
& + 2(\gamma_{10} - \gamma_1)(\gamma_1 - \gamma_{1P}) + (\gamma_{10} - \gamma_{1P})\sin\big(2(\gamma_{1P} - \theta)\big) \\
& + (2\gamma_1 - \gamma_{10} + \gamma_{1P})\sin\big(2(\gamma_1 - \theta)\big) + \cos\big(2(\gamma_1 - \theta)\big) \\
& - \cos\big(2(\gamma_{1P} - \theta)\big)\Big]\Big\}
\end{aligned}
\tag{93}
$$

When evaluated for a given wheel position, Equations (91) and (93) are inserted into the hull equations of motion, while Equation (92) is inserted into the wheel equations of motion as shown below.

2. Integrations Involving Shear Stress

As in the rigid wheel case, the expressions for $F_{x\tau}$, $F_{z\tau}$, M_τ, and $M_{x\tau}$ are not easily integrable. Again, a numerical solution is the best approach in this case. When evaluated, these force and moment terms are inserted into the equations of motion in a manner similiar to that for normal stress.

H. EQUATIONS OF MOTION IN THE SIMULATION

With the soil forces and moments just derived, Equations (8), (9), (10), (11), and (12) can now be used to specify the particular equations of motion for the system used in the simulation. Figure 18 shows

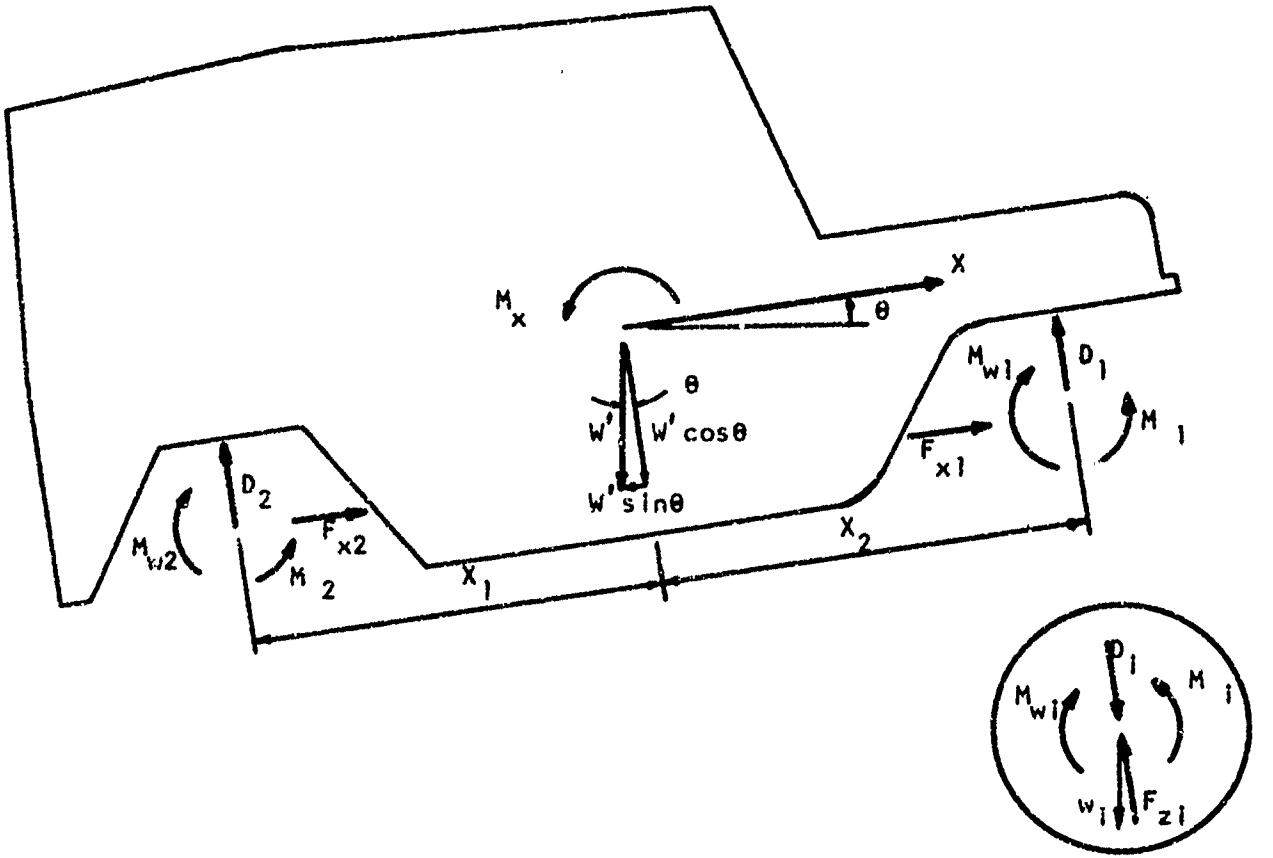

FIGURE 18 FORCES AND MOMENTS ON THE VEHICLE AND WHEELS

the vehicle with the forces and moments acting on it. From Figure 18, and Equations (8), (9), and (10), the hull equations are

$$\ddot{X}_{CG} + \dot{\theta}\dot{Z}_{CG} = \frac{1}{M}\left[F_{x1} + F_{x2} - W' \sin\theta\right] \tag{94}$$

$$\ddot{Z}_{CG} - \dot{\theta}\dot{X}_{CG} = \frac{1}{M}\left[W' \cos\theta - D_1 - D_2\right] \tag{95}$$

$$I_y\ddot{\theta} = D_1X_1 - D_2X_2 + M_{T1} + M_{T2} - M_{w1} - M_{w2} \tag{96}$$

where

D_1 and D_2 are suspension forces

$F_x = F_{x\sigma} + F_{xT}$

M_w = the engine torque on a wheel

the subscripts denote front and rear wheels

Figure 18 also shows a wheel with the forces and moments acting on it. From Figure 18, and Equations (11) and (12), the wheel equations are

$$\ddot{z}_1 - \dot{\theta}_w\dot{X}_{CG} = \frac{1}{m_1}\left[w_1 \cos\theta + D_1 - F_{z1}\right] \tag{97}$$

$$\ddot{z}_2 - \dot{\theta}_w\dot{X}_{CG} = \frac{1}{m_2}\left[w_2 \cos\theta + D_2 - F_{z2}\right] \tag{98}$$

$$I_{yw}\ddot{\theta}_w = M_{w1} + M_{w2} - M_{T1} - M_{T2} \tag{99}$$

where

$\dot{\theta}_w$ = the angular velocity of the wheels (the same for all wheels)

$F_z = F_{z\sigma} + F_{zT}$

Note that the signs of M_w and M_T are reversed from the hull equations, since for the wheel, clockwise rotation is positive.

IV. THE SIMULATION

A. GENERAL

The model in this report was developed as part of a simulation in a larger project headed by Dr. M. Peter Jurkat, Davidson Laboratory, Stevens Institute of Technology. The simulation used as a subroutine a program which the author wrote to determine the forces and moments on the vehicle due to the wheel-soil interaction.

B. CONCEPT

Unbalanced forces are calculated as a result of vehicle velocity, and wheel position with respect to the vehicle and the ground. These unbalanced forces are used to move the vehicle to a new position and velocity via the equations of motion.

At the beginning of the simulation, initial position and velocity are assigned to the vehicle. This position determines the amount of wheel-soil interferance in terms of the exit and entry angle of the wheel. Using these and the soil parameters, Equations (34), (35), (37), (38), (55), (56), and (57) calculate the forces and moments derived in Section III for the rigid wheel case. If the flexible wheel case obtains, Equations (84), (85), (86), (90), (91), (92), and (93) are used. These forces and moments are then inserted into the equations of motion, which are numerically integrated to get a new position, velocity, and acceleration. The process is then repeated.

C. DESCRIPTION

The simulation program consists of five major subroutines, which are shown in block diagram in Figure 19. The simulation is quite

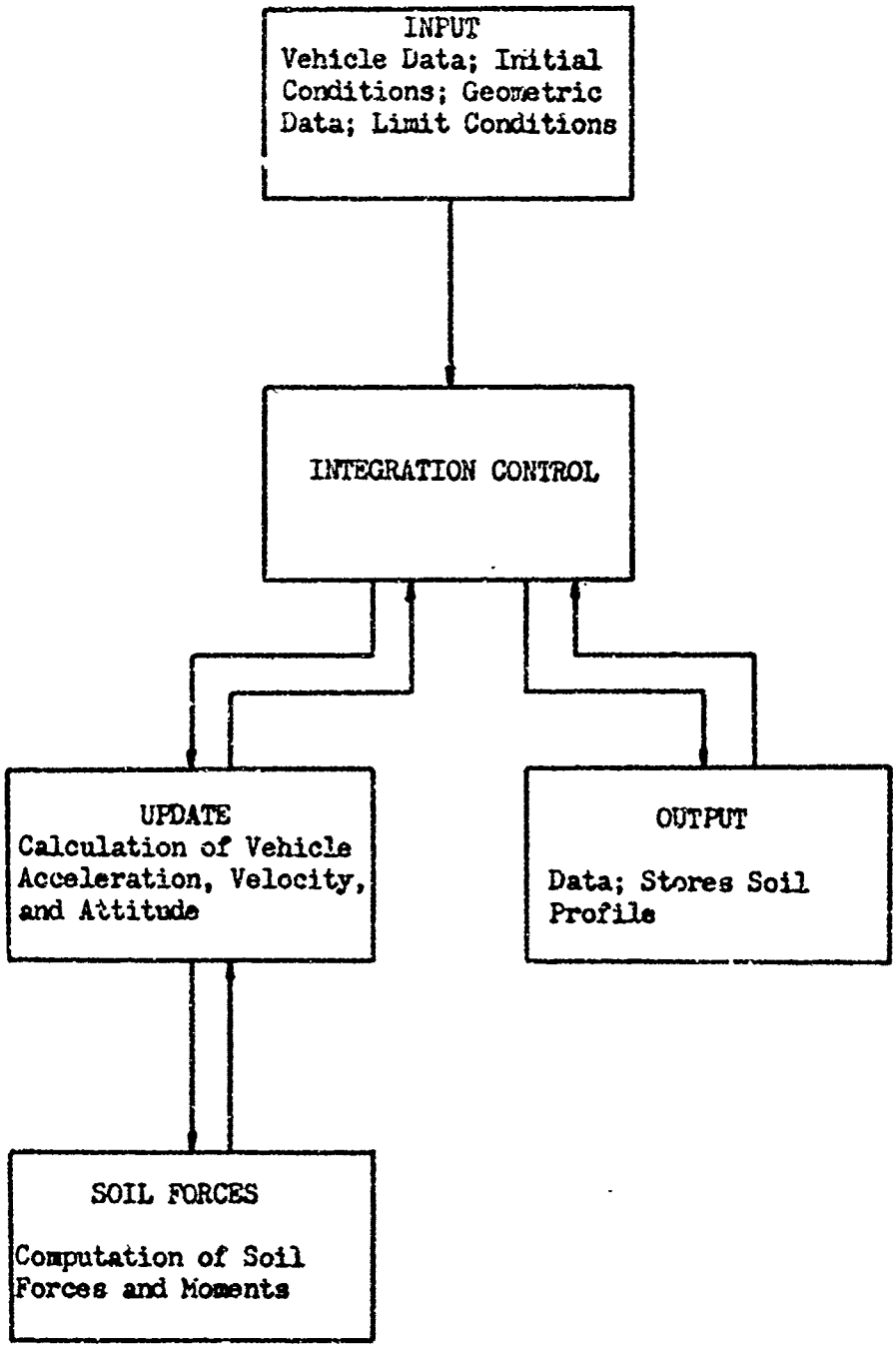

FIGURE 19 PROGRAM SUBROUTINES

flexible with respect to types of vehicles, soil parameters, and ground profiles which may be used. A description of the subroutines, with comments on their capabilities, follows.

INPUT

(1) Reads vehicle description; the vehicle sprung weight, unsprung weight, moment of inertia, location of CG, etc., must be specified.

(2) Reads soil profile and parameters. The program stores the soil profile as coordinate locations, so any profile can be used. The soil parameters can be varied along the profile to simulate changing soil conditions which the prototype might encounter.

(3) Reads initial conditions of the problem. The vehicle can be started from rest, or with an initial velocity.

(4) Positions vehicle with respect to the soil profile.

(5) Reads integration control variables.

INTEGRATION CONTROL

(1) Calls a subroutine which integrates the equations of motion by the Hamming Predictor-Corrector Method.

(2) Tests for completion of simulation.

UPDATE

(1) Calculates wheel position with respect to soil profile in terms of Y_1, Y_{10}, and Y_8.

(2) Calculates local ground slope and wheel slip.

(3) Calls soil force subroutine.

(4) Calculates engine torque; checks engine torque vs RPM map and shifts to proper transmission gear.

(5) Calculates suspension forces.

(6) Calculates accelerations in all degrees of freedom from the equations of motion.

OUTPUT

(1) Prints results.

(2) Modifies soil profile due to wheel-soil interference. Stores current and original soil profiles.

SOIL FORCES

(1) Calculates wheel sinkage and theoretical maximum soil pressure.

(2) Determines whether rigid wheel of flexible wheel case holds.

(3) Calculates soil forces and moments derived in Section III.

V. QUALITATIVE VALIDATION

Since no experimental data exists which relates vehicle performance to soil parameters, the model was "validated" on a qualitative basis. It is generally expected that vehicle performance will increase as soil strength increases. To determine if the model did produce results with this trend, the following approach was selected:

- Part 1

1. Select c, k_c, n, K, ϕ, and a uniformly sloping soil profile.

2. Vary k_ϕ to change soil strength.

3. Use the ability of the vehicle to climb the slope as a measure of the effect of soil strength.

- Part 2

For a soil strength which allows the vehicle to just climb the slope, change the per cent of slope and examine its effect on vehicle performance.

For the first portion of the validation, the soil selected was a cohesionless one with the following parameters:

$$c = 0$$

$$k_c = 0$$

$$n = 1$$

$$K = 0.2$$

$$\tan\phi = 0.28$$

A 15% slope was selected. Values of k_ϕ chosen were 30, 40, and 50. The higher values of k_ϕ relate to stronger soil, as seen from Equations

(44) and (51). The initial velocity selected was 60 inches per second, or 3.4 miles per hour.

Table 2 shows the vehicle velocity at 0.1 second intervals for each case. Figure 20 is a plot of velocity vs time for each case. The first 1.5 seconds is considered the transient portion of the simulation; it arises from the assignment of initial conditions which are not steady-state. For a k_ϕ of 30, the vehicle could not continue to climb the slope, and the velocity gradually decreased. At a k_ϕ of 40, the vehicle was able to slightly accelerate up the slope. At a k_ϕ of 50, the vehicle was able to accelerate even more. Thus, as soil strength increased, vehicle performance increased as expected.

For the second portion of the validation, the value of 40 for k_ϕ was selected. The simulation was executed for values of slope of 17.5% and 20%. Table 3 shows the vehicle velocity at 0.1 second intervals for each case. The plot in Figure 21 shows that as slope is increased, vehicle performance decreases as expected.

TABLE 2

VEHICLE VELOCITY AT SELECTED TIMES FOR VARIOUS k_ϕ

TIME (sec)	VELOCITY (in/sec)		
	$k_\phi = 30$	$k_\phi = 40$	$k_\phi = 50$
0.00	60.00	60.00	60.00
0.10	62.14	60.66	60.84
0.20	60.26	60.46	61.18
0.30	58.58	60.89	62.15
0.40	58.60	61.48	63.27
0.50	58.84	62.07	64.37
0.60	58.90	62.49	65.35
0.70	58.78	62.80	66.09
0.80	58.16	63.07	66.81
0.90	57.47	63.43	67.64
1.00	56.56	63.90	68.46
1.10	56.17	64.31	69.30
1.20	56.01	64.74	70.19
1.30	55.86	65.24	71.40
1.40	55.86	65.93	71.86
1.50	56.55	65.94	72.56
1.60	56.28	66.18	73.27
1.70	54.55	66.38	73.98
1.80	54.03	66.66	74.73
1.90	53.68	66.97	75.48
2.00	53.33	67.27	76.21
2.10	53.05	67.59	76.96
2.20	52.84	67.85	77.62
2.30	52.52	68.12	78.34
2.40	52.22	68.38	78.95
2.50	51.91	68.68	79.64
2.60	51.65	68.96	80.28
2.70	51.32	69.26	81.08
2.80	51.10	69.58	81.84
2.90	50.78	69.91	82.52
3.00	50.46	70.21	83.21

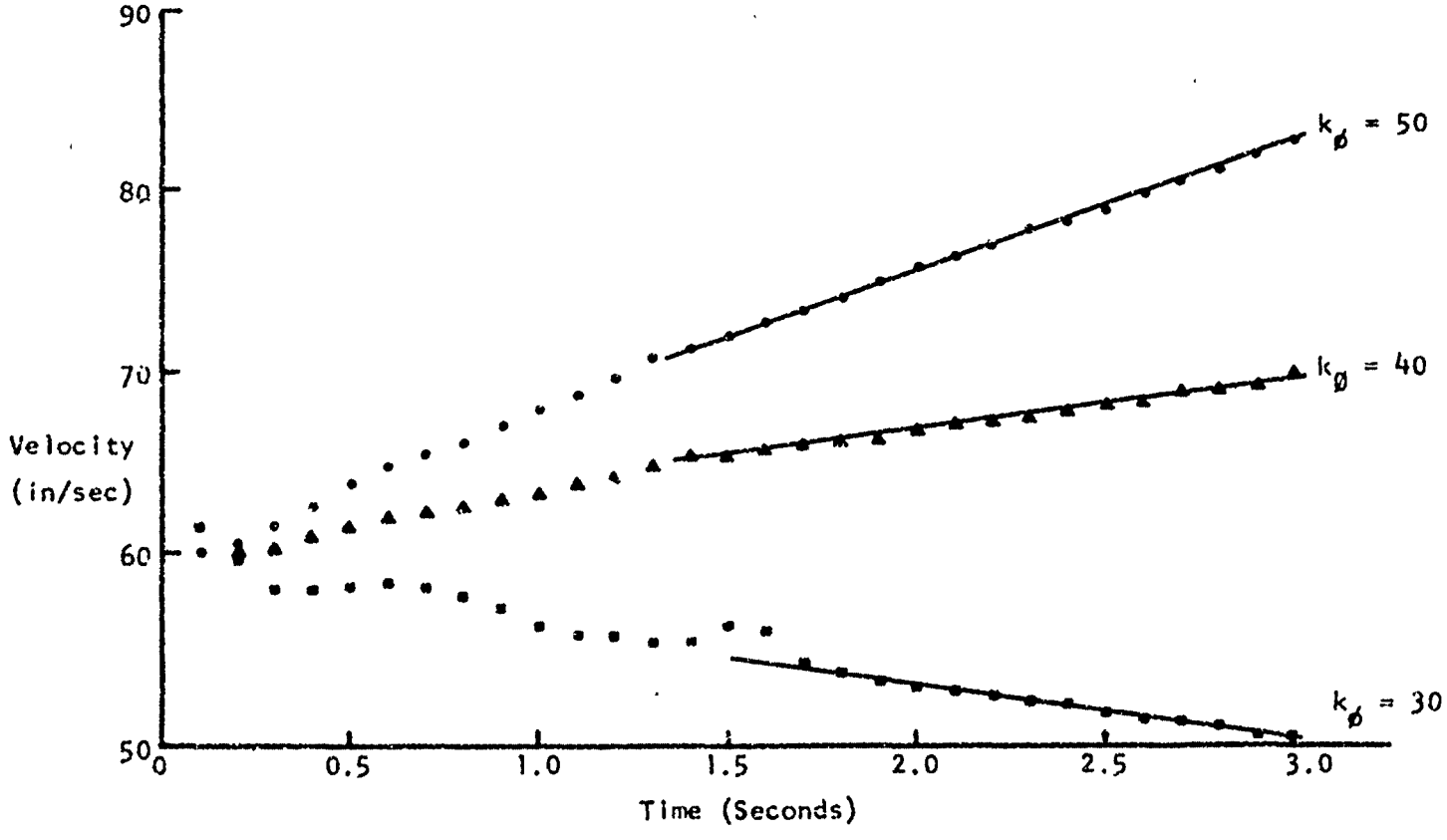

FIGURE 20 PLOT OF VEHICLE VELOCITY VS TIME FOR VARIOUS k_ϕ

TABLE 3

VEHICLE VELOCITY AT SELECTED TIMES FOR VARIOUS SLOPES

TIME (sec)	VELOCITY (in/sec)		
	15% SLOPE	17½% SLOPE	20% SLOPE
0.00	60.00	60.00	60.00
0.10	60.66	60.53	59.57
0.20	60.46	59.09	56.97
0.30	60.89	58.77	55.90
0.40	61.48	58.61	55.15
0.50	62.07	58.50	54.31
0.60	62.49	58.23	53.38
0.70	62.80	57.89	52.28
0.80	63.07	57.48	51.04
0.90	63.43	57.08	49.86
1.00	63.90	56.75	48.78
1.10	64.31	56.47	47.72
1.20	64.74	56.22	46.69
1.30	65.24	55.52	45.65
1.40	65.93	55.18	44.57
1.50	65.94	55.65	43.36
1.60	66.18	54.84	43.11
1.70	66.38	54.22	42.76
1.80	66.66	53.80	40.72
1.90	66.97	53.30	39.22
2.00	67.27	52.80	37.95
2.10	67.59	52.61	36.70
2.20	67.85	51.69	35.48
2.30	68.12	50.98	34.20
2.40	68.38	50.56	33.05
2.50	68.68	50.19	31.43
2.60	68.96	49.84	29.17
2.70	69.26	49.36	27.10
2.80	69.58	49.14	25.61
2.90	69.91	48.12	24.16
3.00	70.21	47.50	22.56

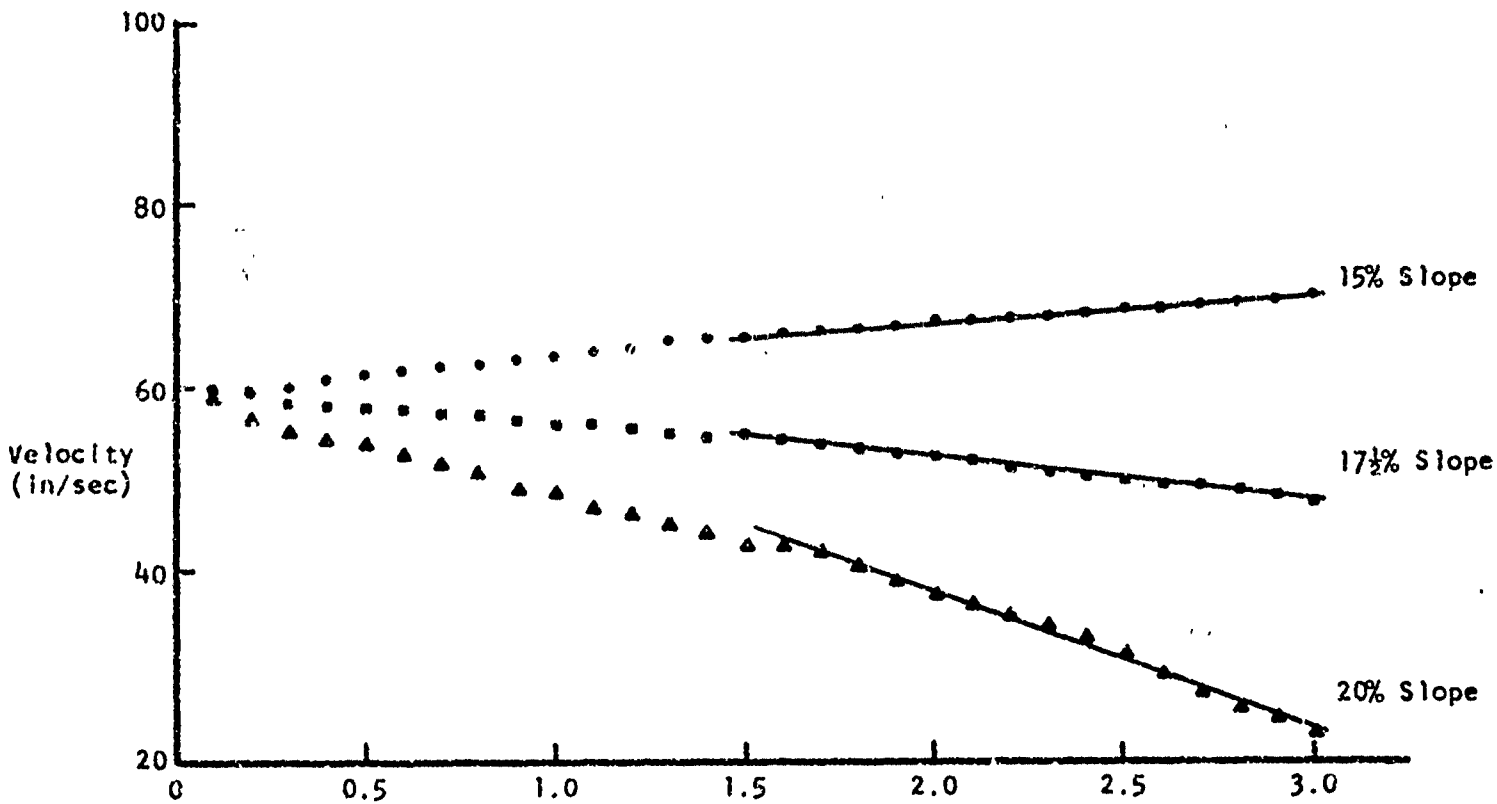

FIGURE 21 PLOT OF VEHICLE VELOCITY VS TIME FOR VARIOUS SLOPES

VI. CONCLUSIONS AND RECOMMENDATIONS

A. CONCLUSION

On a qualitative basis, the model of vehicle dynamics and wheel-soft soil interaction presented in this study is a valid simulation of actual vehicle performance.

B. RECOMMENDATIONS

1. That experimental data be gathered to assess the validity of the model on a quantitative basis.

2. That the equations of motion presented in this study be modified to include the relative accelerations of the wheels discussed in Section III.B.

3. That the soil-wheel equations presented be modified to use the Sela-Ehrlich improved equations for normal stress.

REFERENCES

1. Schuring, D., and Belsdorf, M. R., Analysis and Simulation of Dynamical Vehicle-Terrain Interaction, Cornell Aeronautical Laboratory Technical Memorandum Nº VJ-2330-G-56, Buffalo, NY, May 7, 1969.

2. Muddappa, S. D., and Baker, Warren J., Egress Performance of Amphibious Vehicles, University of Detroit Technical Report, Detroit, Michigan, August 1, 1971.

3. Gloss, D., Ehrlich, I. R., and Worden, G., Studies of Off-Road Vehicles in the Riverine Environment (Volume II, An Analytical Method for Egress Evaluation), Davidson Laboratory Report 1393, Hoboken, New Jersey, October 1969.

4. Schoch, D. F., and Shah, R. F., Dynamic Modeling of Military Ground Vehicles, U. S. Army Tank Automotive Command Technical Report Nº 11462, Warren, Michigan, November 1971.

5. Bekker, M. G., Off Road Locomotion, Ann Arbor; University of Michigan Press, 1960.

6. Sela, A. D., and Ehrlich, I. R., Load Support Capability of Flat Plates of Various Shapes in Soils, Society of Automotive Engineers Paper 710178, New York, January, 1971.

7. Sela, A. D., and Ehrlich, I. R., Prediction of Rigid Wheel Performance From Plate Sinkage Tests, Davidson Laboratory Report 1531, Hoboken, New Jersey, September 1971.

8. Taylor, D. W., Fundamentals of Soil Mechanics, New York; John Wiley & Sons, Inc., 1948.

9. Janosi, Z., and Hanamoto, B., The Analytical Determination of Drawbar Pull as a Function of Slip for Tracked Vehicles in Deformable Soils, Proceedings of the First International Conference on the Mechanics of Soil-Vehicle Systems, Paper Nº 44, Editzione Minerva Technica, Turin, Italy, 1962.

10. Janosi, Z. J., An Analysis of Pneumatic Tire Performance on Deformable Soil, Proceedings of the First International Conference on the Mechanics of Soil-Vehicle Systems, Paper Nº 45, Editzione Minerva Technica, Turin, Italy, 1962.

11. Etkin, Bernard, Dynamics of Flight, New York; John Wiley & Sons, Inc., 1959.

12. Ehrlich, I. R., Wheel Sinkage in Soils, Ph.D. Dissertation, University of Michigan, 1960.

13. Karafiath, L. L., Nowatzke, E. A., Ehrlich, I. R., and Capin, J., An Application of Plasticity Theory to the Solution of the Rigid Wheel-Soil Interaction Problem, U. S. Army Tank Automotive Command Technical Report № 11758, Warren Michigan, March 1973.

14. Bekker, M. G., Introduction to Terrain-Vehicle Systems, Ann Arbor; University of Michigan Press, 1969.

15. Ellis, J. R., Vehicle Dynamics, London; Business Books Limited, 1969.

ACKNOWLEDGEMENTS

I wish to thank my advisor, Dr. I. Robert Ehrlich, Research Assistant Professor of Mechanical Engineering, for providing guidance and a sense of direction to this study.

I also wish to thank Dr. M. Peter Jurkat, Chief, Motor Vehicle and Traffic Research Division, Davidson Laboratory, who guided me through the Labyrinth of FORTRAN programming, reviewed and commented on my work as the study progressed, and, most importantly, developed the simulation which allowed me to test my model.

I would also like to extend a special note of appreciation to Stevens Institute of Technology, which provided the funds for the computer time used during this study.

VITA

CPT SHERIDAN L MISZKLEVITZ was born 16 January 1943 in Troy, Ohio. He attended Purdue University, where he was awarded a Bachelor of Science Degree in Civil Engineering, and was commissioned a Second Lieutenant in the United States Army, in June of 1966. In December of that year, he married Norma Lynn 'nee Galbreath.

Cpt Miszklevitz has been on active duty in the US Army since August of 1966. After brief schooling at Aberdeen Proving Ground, Maryland, he was assigned to Okinawa for 29 months. After that, he spent a year in Viet Nam. From there, it was back to Aberdeen for 9 more months of military schooling before coming to Stevens. Cpt Miszklevitz's experience in the Army has been mainly in the field of Ammunition Supply; he has worked at Company, Battalion, and Depot level.